

1 **Title:**

2 **The Impact of SIV-Induced Immunodeficiency on Clinical Manifestation, Immune
3 Response, and Viral Dynamics in SARS-CoV-2 Coinfection**

4

5 Alexandra Melton^{1,2}, Lori A Rowe¹, Toni Penney¹, Clara Krzykwa¹, Kelly Goff¹, Sarah
6 Scheuermann¹, Hunter J Melton³, Kelsey Williams¹, Nadia Golden¹, Kristyn Moore
7 Green¹, Brandon Smith¹, Kasi Russell-Lodrigue^{1,4}, Jason P Dufour^{1,4}, Lara A Doyle-
8 Meyers^{1,4}, Faith Schiro¹, Pyone P Aye^{1,4}, Jeffery D Lifson⁵, Brandon J Beddingfield^{1,9},
9 Robert V Blair¹, Rudolf P Bohm^{1,4,6}, Jay K Kolls^{7,8}, Jay Rappaport^{1,9}, James A Hoxie¹⁰,
10 Nicholas J Maness^{1,9,*}

11

12 ¹Tulane National Primate Research Center, Covington, Louisiana

13 ²Biomedical Science Training Program, Tulane University School of Medicine, New
14 Orleans, Louisiana

15 ³Florida State University, Department of Statistics, Tallahassee, Florida

16 ⁴Department of Medicine, Tulane University School of Medicine, New Orleans, Louisiana

17 ⁵AIDS and Cancer Viruses Program, Frederick National Laboratory, Frederick, Maryland,
18 United States of America

19 ⁶Present address: Oregon National Primate Research Center, Oregon Health and
20 Science University, Beaverton, Oregon

21 ⁷Departments of Medicine and Pediatrics, Center for Translational Research in Infection
22 and Inflammation, Tulane University School of Medicine, New Orleans, LA 70112, USA.

1 ⁸Department of Pulmonary Critical Care and Environmental Medicine, Tulane University
2 School of Medicine, New Orleans, LA 70112, USA.

3 ⁹Department of Microbiology and Immunology, Tulane University School of Medicine,
4 New Orleans, Louisiana

5 ¹⁰Perelman School of Medicine, University of Pennsylvania, Philadelphia, Pennsylvania

6 *To whom to address correspondence; nmaness@tulane.edu

7

8 **Abstract:**

9 Persistent and uncontrolled SARS-CoV-2 replication in immunocompromised individuals
10 has been observed and may be a contributing source of novel viral variants that continue
11 to drive the pandemic. Importantly, the effects of immunodeficiency associated with
12 chronic HIV infection on COVID-19 disease and viral persistence have not been directly
13 addressed in a controlled setting. Here we conducted a pilot study wherein two pigtail
14 macaques (PTM) chronically infected with SIVmac239 were exposed to SARS-CoV-2
15 and monitored for six weeks for clinical disease, viral replication, and viral evolution, and
16 compared to our previously published cohort of SIV-naïve PTM infected with SARS-
17 CoV-2. At the time of SARS-CoV-2 infection, one PTM had minimal to no detectable
18 CD4+ T cells in gut, blood, or bronchoalveolar lavage (BAL), while the other PTM
19 harbored a small population of CD4+ T cells in all compartments. Clinical signs were not
20 observed in either PTM; however, the more immunocompromised PTM exhibited a
21 progressive increase in pulmonary infiltrating monocytes throughout SARS-CoV-2
22 infection. Single-cell RNA sequencing (scRNASeq) of the infiltrating monocytes revealed
23 a less activated/inert phenotype. Neither SIV-infected PTM mounted detectable anti-
24 SARS-CoV-2 T cell responses in blood or BAL, nor anti-SARS-CoV-2 neutralizing

1 antibodies. Interestingly, despite the diminished cellular and humoral immune
2 responses, SARS-CoV-2 viral kinetics and evolution were indistinguishable from SIV-
3 naïve PTM in all sampled mucosal sites (nasal, oral, and rectal), with clearance of virus
4 by 3-4 weeks post infection. SIV-induced immunodeficiency significantly impacted
5 immune responses to SARS-CoV-2 but did not alter disease progression, viral kinetics
6 or evolution in the PTM model. SIV-induced immunodeficiency alone may not be
7 sufficient to drive the emergence of novel viral variants.

8

9 **Introduction:**

10 The global outbreak of Coronavirus disease 2019 (COVID-19), caused by the highly
11 infectious severe acute respiratory syndrome coronavirus 2 (SARS-CoV-2), has posed a
12 significant and urgent public health challenge. First identified in Wuhan, China, in
13 December 2019, the outbreak quickly spread to other countries across the globe. As of
14 September 2023, the World Health Organization (WHO) has reported over 770 million
15 global cases and nearly 7 million deaths [1]. While the majority of cases are
16 asymptomatic or exhibit only mild symptoms, some individuals develop severe
17 complications such as pneumonia, systemic inflammation, and coagulopathy, which can
18 lead to organ failure, shock, and death [2–7]. Certain factors, such as a compromised
19 immune system, advanced age, and comorbidities, such as cardiovascular disease,
20 diabetes, and obesity, increase the risk of developing severe disease [8,9].

21

22 People living with HIV (PLWH) face an increased risk of several of these conditions,
23 including a compromised immune system and a higher prevalence of cardiovascular
24 disease. Additionally, PLWH have increased susceptibility to opportunistic infections

1 such as pneumocystis pneumonia, which is the most common respiratory infection in
2 patients with AIDS [10–12]. PLWH also experience elevated levels of inflammation,
3 which significantly contributes to the development of severe respiratory disease,
4 thromboembolisms, and other adverse outcomes associated with COVID-19 [13–15].
5 This raises concerns about the impact of HIV on the severity and persistence of SARS-
6 CoV-2 infections. Studies examining whether HIV increases the risk of severe COVID-19
7 have yielded conflicting results. Initial studies indicated that PLWH had similar or even
8 better outcomes [16–18] compared to those without HIV. However, larger population-
9 based studies suggest that PLWH experience higher hospitalization rates and COVID-
10 19-related deaths compared to the general population [19–23]. More recent research
11 has suggested that unsuppressed viral loads or low CD4+ T cell counts are linked to
12 suboptimal adaptive immune responses to SARS-CoV-2, affecting both T cell and
13 humoral responses [24,25].

14

15 In addition to the concern of increased severity, HIV-associated immunodeficiency could
16 potentially facilitate SARS-CoV-2 persistence and evolution, leading to the emergence of
17 new variants of concern. A recent study by Karim et al. highlighted a case of an
18 individual with advanced HIV who exhibited prolonged SARS-CoV-2 shedding with high
19 viral loads and the emergence of multiple viral mutations [26]. While retrospective
20 studies have explored the effects of HIV status on COVID-19 incidence and severity,
21 controlled studies are lacking. To explore the feasibility of using an NHP model to
22 address these gaps, we conducted a pilot study involving two pigtail macaques (PTM)
23 chronically infected with SIVmac239. We exposed them to SARS-CoV-2 and monitored
24 the animals for six weeks for clinical disease, viral replication, and viral evolution.
25 Additionally, we performed detailed analyses of innate and adaptive immune responses,

1 utilizing flow cytometry, cytokine/chemokine analysis, antibody binding and neutralization
2 assays, and longitudinal single-cell RNA sequencing (scRNA-Seq) of bronchoalveolar
3 lavage (BAL) cells following SARS-CoV-2 infection. We compared our findings with data
4 from our previously published cohort of SIV-naïve, SARS-CoV-2-infected PTMs [27].
5 Despite the marked decrease in CD4+ T cells in the SIV+ animals prior to exposure to
6 SARS-CoV-2, we found that disease progression, viral persistence, and evolution of
7 SARS-CoV-2 were comparable to the control group. Overall, our findings suggest that
8 SIV-induced immunodeficiency alters the immune response to SARS-CoV-2 infection,
9 leading to impaired cellular and humoral immunity. However, this impairment does not
10 significantly alter the course of infection. These findings contribute to a deeper
11 understanding of the interplay between immunodeficiency and SARS-CoV-2 infection
12 and propose a valuable model for evaluating vaccine and therapeutic strategies for
13 immunocompromised individuals.

14

15 **Materials and Methods:**

16 Research Animals

17 Two female pigtail macaques (PTM, Table 1) were inoculated intravenously with
18 SIVmac239 (100 TCID50), followed by intranasal (0.5 mL per nare) and intratracheal (1
19 mL) administration of SARS-CoV-2 (1.1×10^6 PFU/mL, USA WA1/2020) approximately
20 one year later. Animals were monitored for six weeks following SARS-CoV-2 inoculation.
21 Blood, bronchoalveolar lavage (BAL), and endoscopic gut biopsies were collected before
22 and after SIVmac239 infection. Sampling pre- and post-SARS-CoV-2 infection included
23 blood, BAL, and mucosal swabs (nasal, pharyngeal, and rectal). Physical examinations
24 were performed throughout the course of the study. At the end of the study, complete

1 postmortem examinations were performed with collection and histopathologic evaluation
2 of 43 different tissues including all major organs and sections from each major lung lobe.

Animal ID	Sex	Age (y)	Weight (kg) at time of SIV inoculation	Weight (kg) at time of SARS-CoV-2 inoculation
NV18	Female	3.82	4.45	4.45
NV19	Female	4.67	5.76	5.85

3 Table 1. Cohort of PTM used in this study.

4

5 Ethics Statement

6 Pigtail macaques used in this study were purpose bred at Johns Hopkins University and
7 moved to Tulane National Primate Research Center (TNPRC) for these experiments.

8 Macaques were housed in compliance with the NRC Guide for the Care and Use of
9 Laboratory Animals and the Animal Welfare Act. Animal experiments were approved by
10 the Institutional Animal Care and Use Committee of Tulane University. The TNPRC is
11 fully accredited by AAALAC International (Association for the Assessment and
12 Accreditation of Laboratory Animal Care), Animal Welfare Assurance No. A3180-01.

13 Animals were socially housed indoors in climate-controlled conditions with a 12/12-
14 light/dark cycle. All the animals on this study were monitored twice daily to ensure their
15 welfare. Any abnormalities, including those of appetite, stool, behavior, were recorded
16 and reported to a veterinarian. The animals were fed commercially prepared monkey
17 chow twice daily. Supplemental foods were provided in the form of fruit, vegetables, and
18 foraging treats as part of the TNPRC environmental enrichment program. Water was
19 available at all times through an automatic watering system. The TNPRC environmental
20 enrichment program is reviewed and approved by the IACUC semi-annually.

21 Veterinarians at the TNPRC Division of Veterinary Medicine have established
22 procedures to minimize pain and distress through several means. Monkeys were

1 anesthetized with ketamine-HCl (10 mg/kg) or tiletamine/zolazepam (3-8 mg/kg) prior to
2 all procedures. Preemptive and post procedural analgesia (buprenorphine 0.03 mg/kg IM
3 or buprenorphine sustained-release 0.02 mg/kg SQ) was required for procedures that
4 would likely cause more than momentary pain or distress in humans undergoing the
5 same procedures. The animals were euthanized at the end of the study using methods
6 consistent with recommendations of the American Veterinary Medical Association
7 (AVMA) Panel on euthanasia and per the recommendations of the IACUC. Specifically,
8 the animals were anesthetized with tiletamine/zolazepam (8 mg/kg IM) and given
9 buprenorphine (0.01 mg/kg IM) followed by an overdose of pentobarbital sodium. Death
10 was confirmed by absence of respiration, cessation of heartbeat, pupillary dilation, and
11 lack of corneal reflex. The TNPRC policy for early euthanasia/humane endpoint was
12 included in the protocol in case those circumstances arose.

13

14 Isolation and Quantification of SIVmac239

15 Plasma SIVmac239 viral RNA (vRNA) extraction and quantification were performed
16 essentially as previously described [28].

17

18 Isolation of SARS-CoV-2 RNA

19 SARS-CoV-2 vRNA was isolated from BAL supernatant (200 μ L) and mucosal swabs
20 (nasal, pharyngeal, and rectal) using the Zymo Quick-RNA Viral Kit (Zymo Research,
21 USA) as previously described [27,29]. Mucosal swabs, collected in 200 μ L DNA/RNA
22 Shield (Zymo Research, USA), were placed directly into the Zymo spin column for
23 centrifugation to ensure complete elution of the entire volume. The Roche high pure viral
24 RNA kit (Roche, Switzerland) was used to isolate vRNA from plasma (200 μ L) per the

1 manufacturer's protocol. After isolation, samples were eluted in 50 μ L DNase/RNase-
2 free water (BAL and mucosal swabs) or Roche elution buffer (plasma) and stored at -80
3 $^{\circ}$ C until viral load quantification.

4

5 Quantification of SARS-CoV-2 RNA

6 The quantification of SARS-CoV-2 RNA was performed according to methods previously
7 described [27,29]. Genomic vRNA was quantified using CDC N1 primers/probe to
8 determine the total amount of vRNA present. Additionally, primers/probe specific to
9 nucleocapsid subgenomic (SGM) vRNA were utilized to estimate the quantity of
10 replicating virus.

11

12 Meso Scale Panels

13 To measure concentrations of various chemokine and cytokine protein targets, three V-
14 plex MSD Multi-Spot Assay System kits were utilized: Chemokine Panel 1 (Eotaxin, MIP-
15 1 β , Eotaxin-3, TARC, IP-10, MIP-1 α , IL-8, MCP-1, MDC, and MCP-4), Cytokine Panel 1
16 (GM-CSF, IL-1 α , IL-5, IL-7, IL-12/IL-23p40, IL-15, IL-16, IL-17A, TNF- β , and VEGF-A),
17 and Proinflammatory Panel 1 (IFN- γ , IL-1 β , IL-2, IL-4, IL-6, IL-8, IL-10, IL-12p70, IL-13,
18 and TNF- α) (Meso Scale Diagnostics, USA). Protein targets were measured in BAL
19 supernatant (BAL SUP) and EDTA plasma following the manufacturer's instructions, with
20 an extended incubation time of overnight at 4 $^{\circ}$ C to enhance sensitivity. Plasma samples
21 were diluted 4-fold (Chemokine Panel 1) or 2-fold (Cytokine Panel 1 and
22 Proinflammatory Panel 1) in the diluent provided in each kit. The plates were washed
23 three times before adding prepared samples and calibrator standards. The plates were

1 then sealed and incubated on a shaker at room temperature for two hours. Plates were
2 immediately transferred to 4°C for overnight storage. The following day, plates underwent
3 three washes before the addition of detection antibody cocktails. Plates were then
4 sealed and incubated on a shaker for two hours at room temperature. Following three
5 final washes, MSD Read Buffer T was added to the plates, which were immediately read
6 using a MESO QuickPlex SQ 120MM instrument (Meso Scale Diagnostics, USA). The
7 concentration of each analyte was determined based on the standard curve plotted
8 between known concentrations of calibrators and their respective signals. The Pheatmap
9 package in R was used to generate the heatmap depicting log2 fold changes in
10 chemokine and cytokine expression normalized to baseline (pre-SARS-CoV-2
11 inoculation).

12

13 Isolation of Cells

14 SepMate-50 Isolation tubes (Stem Cell Technologies, Vancouver, Canada) were used
15 according to the manufacturer's protocol to isolate peripheral blood mononuclear cells
16 (PBMCs) from whole blood. BAL samples were centrifuged at 1800 rpm at room
17 temperature for 5 minutes. BAL supernatant was collected and stored at -80°C. BAL cell
18 pellets were washed with PBS supplemented with 2% FBS. Tissue-specific lymphocytes
19 were isolated from endoscopic duodenal pinches collected during the SIV portion of the
20 study. Finely cut tissue pieces were added to a T-25 tissue culture flask and incubated in
21 25 mL Hanks Balanced Salt Solution (HBSS, Corning, USA) supplemented with 1mM
22 EDTA (Invitrogen, USA) for 30 minutes at 37°C at 400 rpm. After supernatant removal,
23 samples underwent a second digestion in 25 mL RPMI (Gibco, USA) supplemented with
24 5% FBS, Collagenase II (60 units/mL, Sigma-Aldrich, USA), penicillin/streptomycin (100

1 IU/mL, Gibco, USA), 2 mM glutamine (Gibco, USA), and 25 mM HEPES buffer (Gibco,
2 USA) for 30 minutes at 37°C at 400 rpm. Samples were filtered through a 70-µm sterile
3 cell strainer, washed, and resuspended in PBS with 2% FBS. Nexcelom's Cellometer
4 Auto 2000 (Nexcelom, USA) was used to count the cells. PBMCs were cryopreserved at
5 approximately 1x10⁷ cells/mL in Bambanker cell freezing medium (GC Lymphotec,
6 Japan).

7

8 Flow Cytometry

9 Whole blood, thawed cryopreserved PBMCs, and freshly isolated cells from BAL and gut
10 were washed with PBS supplemented with 2% FBS and stained with fluorescently
11 labeled antibodies against markers listed in the Supplemental Section (S1 Table) as
12 previously described [27]. Briefly, cells were incubated in Live/Dead stain cocktail (50 µL
13 PBS + 0.5 µL live/dead stain per test) (Fixable Aqua Dead Cell Stain Kit, Invitrogen,
14 Lithuania) in the dark for 20 minutes at room temperature. Cells were then washed and
15 incubated in surface-stain cocktail containing 50 µL Brilliant Stain Buffer (BD Bioscience,
16 USA) and antibodies listed in Supplemental Table 1. All samples were run on a BD
17 FACSymphony A5 Cell Analyzer (BD Bioscience, USA), and data were analyzed with
18 FlowJo 10.8.1 for Mac OS X (Tree Star, USA).

19

20 T cell Cytokine Response to SARS-CoV-2

21 Mononuclear cells (MNCs) from blood and BAL were washed, pelleted, and
22 resuspended in DMEM with 1% Anti-Anti and 10% FBS at 1x10⁶ cells/mL. Cells were
23 stimulated overnight at 37°C, 5% CO₂ with either cell stimulation cocktail (Biolegend,

1 USA) or one of the following viral peptide pools obtained through BEI Resources, NIAID,
2 NIH: Peptide Array, SARS Coronavirus Nucleocapsid Protein (NR-52419), Spike
3 Glycoprotein (NR-52402), or Membrane Protein (NR-53822), along with co-stimulatory
4 antibodies (CD28 and CD49d at 1 μ L/mL) and Brefeldin-A (1 μ L/mL, BioLegend, USA).
5 LIVE/DEAD and surface staining was performed as described above. To measure
6 cellular response to viral antigen, cells were washed in PBS containing 2% FBS, fixed
7 and permeabilized with Cytofix/Cytoperm Buffer (BD Biosciences, USA). Cells were
8 incubated in intracellular stain cocktail for 30 minutes at room temperature (S1 Table),
9 washed with 1x BD Perm/Wash Buffer and fixed in 1x BD Stabilizing Fixative (BD
10 Biosciences, Franklin Lakes, NJ).

11

12 Overnight stimulation, surface and intracellular staining of BAL cells isolated from SARS-
13 CoV-2 infected animals were performed under BSL-3 safety conditions. Cells were fixed
14 with 2% Paraformaldehyde for 60 minutes before removal from BSL-3. Samples were
15 run on the BD FACSymphony and analyzed via FlowJo as described above.

16

17 Meso Scale COVID-19 IgA and IgG Panels

18 V-PLEX COVID-19 serological assays were used to quantify serum levels of IgA and
19 IgG binding antibodies to SARS-CoV-2 Spike, Spike N-Terminal Domain (S1 NTD), and
20 Spike Receptor Binding Domain (S1 RBD) (Panel 1, Meso Scale Discovery, USA),
21 following the manufacturer's protocol. Briefly, plates were first incubated at room
22 temperature on a shaker in MSD Blocking solution for 30 minutes, followed by 3 washes
23 with 1X MSD Wash buffer. Plasma samples were diluted 100- (IgA kit) or 1000-fold (IgG
24 kit) and plated in duplicate, along with controls and standards used to generate a seven-

1 point calibration curve. Plates were then sealed and incubated at room temperature on a
2 shaker for 2 hours. Following this, the plates were washed three times before addition of
3 1X detection antibody to each well. After a 1-hour incubation, plates were washed a final
4 3 times, and MSD GOLD Read Buffer B was added to the plates. Plates were read
5 immediately using a MESO QuickPlex SQ 120MM instrument. The concentration of IgA
6 and IgG antibodies was determined using the standard curve generated by plotting the
7 known concentrations of the standards and their corresponding signals.

8

9 SARS-CoV-2 Microneutralization (PRMNT) Assay

10 A microneutralization assay (PRMNT) adapted from Amanat et al. 2020 [30] was used to
11 assess the presence of neutralizing antibodies in serum of SIV+ and SIV naïve SARS-
12 CoV-2 infected PTMs. Vero/TMPRSS2 cells (JCRB Cell Bank, Japan) were seeded in
13 96-well tissue culture-treated plates to be subconfluent at the time of assay. Serum
14 samples were diluted in dilution buffer (DMEM, 2% FBS, and 1% Anti-Anti) to an initial
15 dilution of 1:5, followed by six 3-fold serial dilutions. SARS-CoV-2 (WA1/2020, BEI, USA)
16 was diluted 1:3000 in dilution buffer and added in equal proportions to the diluted sera
17 under Biosafety Level 3 (BSL-3) conditions. Samples were then incubated at room
18 temperature for 1 hour. The culture media was removed from the 96-well Vero cell
19 culture plates, and 100 µL of the virus/sera mixture was added to each well. Dilution
20 buffer and diluted virus (1:6000) were used as the negative and positive controls,
21 respectively. Plates were then incubated for 48 hours at 37°C and 5% CO₂. After the
22 incubation period, the medium was removed, and 100 µL of 10% formalin was carefully
23 added to each well. The plates were allowed to fix overnight at 4°C before being
24 removed from the BSL-3 facility.

1

2 The staining of the plates was conducted under BSL-2 conditions. After carefully
3 removing the formalin, the cells were washed with 200 μ L PBS, followed by the addition
4 of 150 μ L of permeabilization solution (0.1% Triton/PBS). Plates were then incubated at
5 room temperature for 15 minutes. Following the incubation, the cells were washed with
6 PBS and blocked with 100 μ L of blocking solution (2.5% BSA/PBS) for 1 hour at room
7 temperature. After removing the blocking solution, 50 μ L of the primary antibody (SARS-
8 CoV-2 Nucleocapsid Antibody, Mouse Mab, Sino Biologicals, #40143-MM08) diluted
9 1:1000 in 1.25% BSA/PBS was added to each well, followed by a 1-hour incubation at
10 room temperature. The plates were then washed twice with PBS, decanted, and gently
11 tapped on a paper towel to ensure complete antibody removal. Next, 100 μ L of the
12 secondary antibody, Goat anti-Mouse IgG (H+L) Cross-Adsorbed Secondary Antibody
13 (Invitrogen, #A16072) diluted 1:3000 in 1.25% BSA/PBS was added to each well. The
14 plates were incubated for 1 hour at room temperature. Following the incubation period,
15 cells were washed as described above. To initiate color development, 100 μ L of 1-Step
16 Ultra TMB-ELISA developing solution (Thermo Scientific, #34028) was added to each
17 well. The plates were then incubated in the dark at room temperature for 10 minutes. To
18 stop the reaction, 50 μ L of 1N sulfuric acid was added to each well. The optical density
19 was measured and recorded at 450 nm on a Tecan Sunrise Microplate Reader (Tecan,
20 Switzerland). The averages of the positive control wells and negative control wells were
21 calculated separately, and percent inhibition was calculated for each well.

22

23 Single-Cell RNA Sequencing (scRNAseq) of BAL Cells

1 For single-cell sequencing of bronchoalveolar lavage (BAL) cells, we collected samples
2 before SARS-CoV-2 inoculation and on days 2, 7, 21, and 28 post-challenge. BAL
3 samples were centrifuged at room temperature for 5 minutes at 1800 rpm, and the
4 resulting cell pellets were resuspended in DMEM supplemented with 10% FBS and 1%
5 Anti-Anti. We used the Parse Biosciences cell fixation kit following the manufacturer's
6 instructions for PBMCs to fix the cells (Parse Biosciences, USA). Specifically, we fixed 1
7 million cells per animal/timepoint in a 15 mL falcon tube. The fixed cells were stored at -
8 20°C until all samples were collected.

9

10 To enable multiplexing of samples, the Parse Single-cell whole transcriptome kit, which
11 utilizes a combinatorial barcoding approach (Evercode WT, Parse Biosciences, USA),
12 was employed. This allowed us to barcode and multiplex 10 samples collected from the
13 coinfecting animals across five timepoints. For analysis of the processed cells, we
14 conducted two separate runs: the first run included approximately 15,000 cells, while the
15 second run consisted of approximately 42,000 cells. The sublibraries from each run were
16 pooled and sequenced on an Illumina NextSeq 2000 platform, yielding an average depth
17 of 27,165 reads per cell for the first batch and 29,088 reads per cell for the second.

18

19 Analysis of Single-Cell RNA Sequencing Data

20 For analysis of the single-cell sequencing data, we utilized the Parse Biosciences
21 pipeline (v1.0.4.) to generate cell-gene matrix files using concatenated GTF annotations
22 for the Rhesus macaque genome (*Macaca mulatta*, GCA_003339765.3), SARS-CoV-2
23 genome (GCA_009858895.3) and SIV genome (GenBank Accession # M33262.1).
24 Subsequently, the scRNASeq data analysis was performed using the Seurat package in

1 R [31]. The *cell-gene matrix* (DGE.mtx), *cell metadata* (cell_metadata.csv), and *all genes*
2 *files* (all_genes.csv) generated from both experimental runs using the Parse Biosciences
3 pipeline were imported into R using the readMM and read.delim functions. Seurat
4 objects were then created for each run, and the raw count matrices were merged using
5 the merge command.

6

7 To ensure data quality, cells with more than 5% mitochondrial genes, fewer than 200
8 genes, or more than 2500 genes were excluded from further analysis. The data were
9 normalized and scaled using the NormalizeData and ScaleData functions following the
10 standard Seurat workflow. To account for batch effects and biological variability, we
11 applied the Harmony [32] algorithm, which integrates the data by clustering cells based
12 on their cell type rather than specific dataset conditions. Uniform manifold approximation
13 and projection (UMAP) dimensional reduction was performed on the integrated Seurat
14 object, using 20 dimensions based on the Harmony embeddings. Louvain clustering with
15 a resolution of 0.5 was then conducted using the FindNeighbors and FindClusters
16 functions to identify distinct cell clusters. After determining which cells contained SARS-
17 CoV-2 or SIV transcripts, we excluded Day 2 samples from further analysis due to
18 sample quality for one of the coinfecting animals. After removing Day 2, we followed the
19 same method as described above for quality control and integration.

20

21 Identification of Cell Types

22 Cell type annotation was performed by identifying differentially expressed genes (DEGs)
23 using the FindAllMarkers function, which utilizes the Wilcoxon rank-sum test, to
24 determine significant differences in gene expression. Cell clusters were annotated based

1 on expression of canonical cell marker genes. We identified 24 cell types, including
2 epithelial cells (*TPPP3*), monocytes/macrophages (*MRC1*, *MARCO*), proliferating
3 macrophages (*MRC1*, *MARCO*, *MKI67*, *HMGB2*), T cells (*CD3E*), proliferating T cells
4 (*CD3E*, *MKI67*, *HMGB2*), invariant natural killer T cells (iNKT, *CD3E*, *IL7R*^{hi}), natural
5 killer cells (NK, *NKG2D*), Neutrophils (lineage negative), B cells (*MS4A1*, *CD19*,
6 *CD79A*), plasma cells (*JCHAIN*), mast cells (*HPGE*, *CPA3*, *KIT*), plasmacytoid dendritic
7 cells (pDC, *IRF8*), and myeloid dendritic cells (mDC, *ITGAX*). We used the subset
8 function for subclustering analysis of monocyte/macrophage and T cell clusters. Again,
9 the standard Seurat workflow for quality control and the Harmony algorithm for
10 integration were applied. For the T cell subcluster, the number of dimensions was
11 reduced to 10 in the RunUMAP function, and the resolution for FindClusters function
12 was set to 0.2 to refine the clustering results.

13

14 Differential Gene Expression and Gene Set Enrichment Analysis (GSEA) of
15 Monocyte/Macrophage Subclusters

16 Differential gene expression analysis was conducted among the six
17 monocyte/macrophage subclusters using the FindMarkers function in Seurat. Volcano
18 plots were generated to visualize the results, highlighting genes with an average log2
19 fold change (log2fc) greater than 0.25 or less than -0.25 and a p-value less than 0.05
20 indicating statistical significance. GSEA was performed by ranking the list of DEGs
21 based on their average log2fc. This ranking strategy enables the identification of
22 pathways that show enrichment in our gene set, even when individual genes may not
23 reach statistical significance. By considering the collective contribution of genes, we can
24 uncover upregulated pathways that play a significant role in our analysis. Gene symbols
25 were converted into Entrez IDs using the Metascape [33] website

1 (https://metascape.org). We performed GSEA using the Hallmark [34] gene set from The
2 Broad Institute Molecular Signature Database [35,36] (MSigDB). The msigdbr function
3 was used to import the Hallmark gene set, and GSEA analysis was performed using the
4 fgsea function [37]. Bar graphs were generated to illustrate the net enrichment scores
5 (NES) of significantly enriched pathways within each subcluster using a false discovery
6 rate (FDR) threshold of less than 0.1. The same strategy was applied for Hallmark
7 GSEA, comparing NV18 and NV19 at baseline and 7-dpi with an increased FDR of 0.2.
8 Additionally, we compared days 7, 21, and 28 to baseline for each animal and included
9 both KEGG [38–40] and Hallmark gene sets for GSEA.

10

11 **Results:**

12 Experimental Design and Viral Dynamics in SIV-infected Pigtail Macaques Prior to
13 SARS-CoV-2 Exposure

14 Two female pigtail macaques (PTM, NV18 & NV19) were infected intravenously (iv) with
15 SIVmac239 (100 TCID₅₀) and monitored for approximately one year prior to exposure to
16 SARS-CoV-2 (Wa1/2020, 2.2x10⁶ PFU, in/it) (Fig 1A). SIV viral dynamics in plasma
17 followed the typical pattern, with peak viremia occurring approximately two weeks after
18 infection, followed by a set point of around 1x10⁶ for NV18 and 1x10⁵ for NV19 (Fig 1B).
19 The uncontrolled viremia led to a substantial progressive decrease in CD4+ T cells in all
20 sampled compartments (plasma, BAL, and gut) (Fig 1C-E). Notably, beginning at
21 approximately eight weeks post-SIV infection, NV18 exhibited few to no detectable
22 CD4+ T cells in BAL and gut, and these levels remained persistently low until the time of
23 SARS-CoV-2 exposure. The other animal, NV19 also experienced a decline in CD4+ T

1 cells across all sampled compartments, and although levels began to rebound, they
2 never returned to pre-infection levels.

3

4 Impact of SIV-Induced Immunodeficiency on SARS-CoV-2 Replication and Evolution

5 We then sought to investigate how SIV-induced immunodeficiency affects SARS-CoV-2
6 viral replication and evolution in our PTM model. We hypothesized that the observed
7 immunodeficiency in the SIV-infected PTMs would enhance SARS-CoV-2 viral
8 persistence, thereby increasing the risk of viral evolution. Using qRT-PCR, we tracked
9 viral genomic (Fig 2A-E) and SGM (Fig 2F-J) RNA in mucosal swabs (nasal, pharyngeal,
10 and rectal), BAL supernatant (sup), and plasma for six weeks. We compared viral
11 dynamics in our coinfecting animals with our previously published cohort of SIV-naïve
12 PTMs [27]. Viral dynamics in BAL showed robust viral replication during acute infection
13 in both the SIV+ and the controls with viral levels becoming undetectable in all animals
14 by 21 days post infection (dpi). The coinfecting animals cleared vRNA in the rectal
15 mucosa by 14-dpi, the pharynx by 21-dpi, and the nasal mucosa by 28-dpi. The SIV-
16 naïve animals had low levels of detectable virus in the nasal and rectal mucosa at their
17 study end point of 21-dpi, with no detectable virus in the pharynx or plasma.
18 Furthermore, we were unable to detect genomic or SGM vRNA in plasma in either of the
19 coinfecting animals. Surprisingly, both SIV+ animals cleared SARS-CoV-2, similar to the
20 controls, and the absence of prolonged viral persistence consequently precluded any
21 significant viral evolution, with H655Y being the only spike mutation detected in multiple
22 samples from both coinfecting animals at more than 25% of sequence read, including
23 NV18 nasal and pharyngeal from day 2 and pharyngeal from day 5 and NV19 rectal
24 sample from day 2. However, this mutation was also present at a low frequency in the
25 inoculum, precluding any analysis of intrahost selection.

1

2 Clinical Manifestations and Postmortem Observations in Cointfected PTM

3 Animals cointfected with SIVmac239 and SARS-CoV-2 were closely monitored for six
4 weeks following SARS-CoV-2 inoculation. In line with clinical findings in our previous
5 pigtail study, the cointfected animals exhibited only mild COVID-19 symptoms. This
6 outcome was unexpected given that previous studies have indicated PLWH face a
7 higher risk of severe disease attributed to factors such as low CD4+ T cell counts and
8 uncontrolled viremia, both of which were observed in our SIV+ animals [19–23]. Similar
9 to the controls, no significant changes in body weight, temperature, or blood oxygen
10 saturation levels were observed in the cointfected animals (S1 Fig). Furthermore,
11 thoracic radiographs of the cointfected animals closely resembled those of the control
12 group, revealing only subtle changes consistent with mild to moderate manifestations of
13 COVID-19 (S2 Fig). Upon postmortem examination, both animals demonstrated
14 histopathologic changes consistent with chronic SIV infection. Neither animal had
15 lesions that were attributed to SARS-CoV-2 infection, indicating that lesions had
16 resolved. This resolution of SARS-CoV-2-associated lesions is expected given the six-
17 week post-infection time point, viral clearance in these animals, and what has previously
18 been reported in the NHP model. One animal, NV18, had an opportunistic Pneumocystis
19 infection and SIV syncytial giant cells compatible with simian AIDS (SAIDS).

20

21 Assessment of Cytokine and Chemokine Levels in Blood and BAL Following SARS-
22 CoV-2 Infection of SIV+ PTM

23 To assess the changes in cytokine and chemokine levels in blood and BAL following
24 SARS-CoV-2 infection in the cointfected animals, we utilized the MesoScale V-plex MSD

1 Multi-Spot Assay System (Figs 3 and S3). Similar to findings by Huang et al. [41], who
2 reported elevated plasma concentrations of MIP-1 α , MCP-1, IL-7, IL-10, IP-10, IL-2, and
3 GM-CSF, in hospitalized patients, we observed increased levels of MIP-1 α , MCP-1, IL-7,
4 and IL-10 in BAL supernatant from both coinfecting PTMs at 2-dpi (Figs 3 and S3A-S3C).
5 Additionally, at 7-dpi, the more immunocompromised animal (NV18) exhibited higher
6 levels of IP-10, IL-2, and GM-CSF in BAL supernatant. We also detected increased
7 plasma levels of MIP-1 α and MCP-1 for both animals at 2-dpi. Notably, pulmonary levels
8 of several cytokines and chemokines exhibited a secondary increase at days 21 or 28
9 post-infection (MIP-1 α , MCP-1, IL-7, IL-10, IP-10, IL-2, and GM-CSF). Overall, NV18
10 exhibited higher levels of these markers in the lung, while NV19 tended to have higher
11 levels in the plasma.

12

13 Pulmonary Monocyte Infiltration and Chemokine Dynamics in SARS-CoV-2 Infection
14 Pulmonary inflammatory immune cell infiltration, particularly by
15 monocytes/macrophages, is well characterized in COVID-19 [27,29,42–44]. Chemokines
16 associated with monocyte recruitment in the blood include IP-10, TARC/CCL17, and
17 MCP-1/CCL2 [43]. In our study, we observed elevated levels of these chemokines in
18 plasma at 2-dpi in both animals, accompanied by an increase in monocytes (Figs S3C
19 and 4). Furthermore, NV19 demonstrated increases in these chemokines in BAL
20 supernatant at 2-dpi. Interestingly, the more immunocompromised animal (NV18) initially
21 exhibited a decrease in IP-10 and TARC levels in the lung, followed by a rise at day 7.
22 We also observed pulmonary infiltration of classical monocytes at 2-dpi (NV18 and
23 NV19, Fig 4B) and intermediate monocytes at days 2 (NV18) and 7 (NV19) (Fig 4C).
24 Similar monocyte kinetics were observed in the SIV-naïve animals, with a transient
25 increase in pulmonary infiltrating monocytes during the acute phase of SARS-CoV-2

1 infection, returning close to baseline at approximately 14-dpi. While monocyte kinetics
2 were similar for NV19 and the control animals, NV18 had higher peripheral levels of all
3 monocyte subsets, along with increased pulmonary monocytes at 21 and 28-dpi.
4 Notably, we also observed a spike in several cytokines (IL-6, 1L-10, IL-13, 1L-2, 1L-4,
5 IL-12p70, IL-1B, IL-16, IL-17A, VEG-F, GM-CSF, IL-5, and IL-7) and chemokines
6 (TARC, IL-8, MIP-1B, Eotaxin, Eotaxin-3, MCP-4, MIP-1a, and MIP-1a) in BAL at 28-dpi,
7 suggesting a potential role for these markers in monocyte recruitment and/or function
8 (S3 Fig). It is important to note, however, that due to sample availability constraints, we
9 were unable to conduct the same Meso Scale cytokine/chemokine analyses on the SIV-
10 naïve animals. Given that we lack direct comparison to the SIV-naïve cohort, we are
11 limited in our ability to draw definitive conclusions from our cytokine and chemokine
12 results.

13

14 T cell Dynamics in Blood and BAL Following SARS-CoV-2 Infection

15 T lymphopenia, specifically of CD4+ T cells, is a common feature observed in human
16 COVID-19 patients. This, compounded with low CD4+ T cell counts due to advanced
17 HIV/SIV infection, may delay the clearance of SARS-CoV-2, increase the risk of viral
18 evolution, and promote disease progression [45,46]. In our study, both coinfected
19 animals displayed signs of immunodeficiency with a substantial loss of CD4+ T cells in
20 blood, lung, and gut prior to SARS-CoV-2 exposure (Fig 1C-E). Acutely following SARS-
21 CoV-2 infection, both animals experienced a further decline in peripheral CD4+ T cells.
22 In NV19, this decline was transient and reached a nadir at 2-dpi. However, in the more
23 immunocompromised animal, NV18, the loss persisted, and CD4+ T cells remained
24 undetectable in both blood and BAL for the remainder of the study (Figs 5A, 5C, 5E, and
25 5G). Both animals showed a reduction in the overall CD3+ T cell population in BAL at 2-

1 dpi with levels returning to baseline in NV19 at 7-dpi (Fig 5F). T cell dynamics in the SIV-
2 naïve animals exhibited patterns similar to those of NV19, though with slightly delayed
3 kinetics (Figs 5B-D and 5F-H). Despite the loss of CD4+ T cells, both coinfecte animals
4 successfully cleared SARS-CoV-2, suggesting the involvement of innate immune
5 mechanisms in controlling the infection.

6

7 Diminished Cellular Immune Response to SARS-CoV-2 in Coinfected Animals with
8 Severe T Cell Lymphopenia

9 To evaluate the cellular immune response to SARS-CoV-2 infection, we stimulated
10 mononuclear cells isolated from BAL with peptides derived from SARS-CoV-2 Spike,
11 Membrane, or Nucleocapsid proteins and assessed cytokine responses using flow
12 cytometry. In our previous PTM study, we showed that at 21-dpi, the SIV-naïve animals
13 developed pulmonary CD4+ and CD8+ SARS-CoV-2-specific T cell responses, that
14 were predominately CD4 driven. However, in our current study, neither coinfecte
15 animal had detectable virus-specific cellular immune responses to peptide stimulation
16 (Fig 6). Consistent with our previous findings, we were unable to detect virus-specific T-
17 cell responses in the blood at 21-dpi (S4 Fig). Our findings show that severe CD4+ T-cell
18 lymphopenia, resulting from advanced SIV infection, significantly impairs the cellular
19 immune response to SARS-CoV-2 in the lungs.

20

21 Impaired Humoral Immune Response to SARS-CoV-2 Infection

22 We then aimed to assess neutralization capacity of serum antibodies using a
23 microneutralization assay (PRMNT) [30]. By 14-dpi, the SIV-naïve animals demonstrated
24 detectable neutralizing antibodies against SARS-CoV-2, whereas the coinfecte animals

1 failed to generate a neutralizing antibody response (Fig 7A). Additionally, using the V-
2 PLEX COVID-19 serological assay kit from Meso Scale Discovery, we measured IgA
3 and IgG binding antibody levels in serum. By 21-dpi, we detected IgA (Fig 7B) and IgG
4 (Fig 7C) binding antibodies targeting various domains of the Spike protein, including the
5 receptor binding domain (RBD), Spike S1 and S2 domains, and the Spike N-terminal
6 domain (NTD) in the SIV-naïve PTMs. However, we were unable to detect IgA or IgG
7 binding antibodies in the serum of the coinfecting animals. Our data demonstrate that the
8 coinfecting animals failed to generate virus-specific T cell and humoral immune
9 responses highlighting the impact of pre-existing immunodeficiency on the development
10 of adaptive immunity during coinfection.

11

12 Single-Cell RNA Sequencing

13 To gain a more detailed understanding of the pulmonary immune response to SARS-
14 CoV-2 infection in the coinfecting animals, we conducted single-cell RNA sequencing
15 (scRNAseq) on cells isolated from BAL at baseline (48 weeks post SIVmac239
16 exposure) and days 2, 7, 21, and 28 post-SARS-CoV-2 infection (Fig 8). This approach
17 allowed us to examine the immune response at a higher resolution and capture dynamic
18 changes over the course of coinfection (Figs 8C and 8D). Cell type clusters identified in
19 BAL included monocytes/macrophages, dendritic cells (DC), neutrophils, natural killer
20 (NK) cells, invariant natural killer T (iNKT) cells, T cells, B cells, plasma cells, mast cells
21 (MC), as well as proliferating T cells and macrophages (Figs 8A, 8B, and S5). It should
22 be noted that due to sample availability, we were unable to perform scRNAseq analysis
23 on the SIV-naïve animals therefore the results presented here within should be
24 interpreted as observational.

1

2 Prior to SARS-CoV-2 challenge, the more immunocompromised animal (NV18) exhibited
3 a higher proportion of monocytes/macrophages in the lung, while the other coinfecte
4 animal (NV19) had higher levels of T cells (Figs 8C and 8D). At 7-dpi, both animals
5 experienced an increase in monocytes/macrophages compared to baseline. Notably, the
6 more immunocompromised animal consistently had higher levels of proliferating
7 macrophages at all timepoints. We also observed an increase in neutrophils late in
8 infection at 28-dpi. Following an initial decrease in the proportion of T cells at day 7, T
9 cell levels rebounded to baseline by day 21, with a slight increase observed at 28-dpi.

10 Additionally, B cell levels peaked in both animals at 28-dpi.

11

12 Single-Cell Sequencing Identifies Multiple Cell Types Containing Viral RNA

13 We identified a diverse range of cell types containing viral transcripts by aligning the
14 sequencing reads to the macaque, SARS-CoV-2, and SIV genomes (S6 and S7 Figs).
15 Interestingly, we found SARS-CoV-2 RNA predominantly in DCs (S6B and S6C Figs),
16 while neutrophils contained the highest percentage of SIV RNA (S7B and S7C Figs).
17 The presence of vRNA in these cells can be attributed to various factors, including active
18 viral replication, phagocytosis of infected cells, or potential viral contamination during the
19 processing stages involved in single-cell sequencing [47]. We detected SARS-CoV-2
20 RNA exclusively at 2-dpi (S6D Fig), whereas SIV RNA was detectable at baseline and
21 on days 21 and 28, indicating ongoing viral activity during those timepoints (S7D Fig). It
22 is important to note that due to sample limitations, we only have scRNAseq data for one
23 animal at 2-dpi. Therefore, we excluded the 2-dpi timepoint from any further analysis.

24

1 scRNAseq Reveals Diverse Monocyte/Macrophage Populations in BAL

2 We then used single-cell analysis to gain a deeper understanding of
3 monocyte/macrophage dynamics in BAL during SARS-CoV-2 infection in SIV+ PTMs.
4 Specifically, we performed a subclustering analysis of the “Mono/Mac” cluster depicted
5 in Figure 8A. This analysis revealed six subclusters characterized by variable gene
6 expression patterns (Figs 9, S8A, and S8B). Among these, four populations exhibited
7 features suggestive of alveolar macrophages, while the remaining two displayed
8 characteristics associated with infiltrating/monocyte-derived macrophages. Typical
9 markers of alveolar macrophages include CD68, CD11b (*ITGAM*), CD206 (*MRC1*), and
10 the scavenger receptor class-A marker (*MARCO*). Within these subclusters, we
11 identified resting macrophages [48] (*FABP4*+ *DDX60*-), infiltrating monocytes, anti-
12 inflammatory macrophages [49] (*APOE*^{hi}), *FPR3*^{hi} macrophages, activated macrophages
13 (*IDO1*^{hi}, *CXCL10*^{hi}), and proliferating macrophages (*MKI67*+, *HMGB2*+). The more
14 immunocompromised animal, NV18, exhibited a prominent increase in monocyte-
15 derived cells with a more inert phenotype at 7-dpi, rising from 23% prior to SARS-CoV-2
16 infection to 60% of the total monocyte/macrophage population. This elevation persisted
17 over the remaining 28 days of sampling (Fig 9C, S8A and S8B). While monocyte-derived
18 cells dominated the pulmonary immune landscape of NV18, NV19 demonstrated an
19 increase not only in monocyte-derived cells but also in anti-inflammatory macrophages
20 (*APOE*^{hi}), activated macrophages (*IDO1*^{hi}, *CXCL10*^{hi}), and proliferating macrophages at
21 7-dpi. Levels of all monocyte/macrophage subtypes began to normalize over time in this
22 animal, with only anti-inflammatory macrophages remaining elevated at 28-dpi.

23

24 To gain additional insights into the monocyte/macrophages during coinfection, we
25 performed gene set enrichment analysis (GSEA) on differentially expressed genes

1 (DEGs) comparing the two coinfecting animals at baseline and 7-dpi (Figs S9A and
2 S9B). Prior to SARS-CoV-2 infection, NV18 exhibited enrichment in IFN- γ and IFN- α
3 responses, indicating greater activation of these pathways, potentially due to elevated
4 SIV viremia and SIV-associated disease severity in this animal (S9A Fig). However, at 7-
5 dpi, monocytes/macrophages in the other animal (NV19) showed enrichment in
6 pathways typically upregulated during a respiratory infection, such as TNF- α and IL-6
7 signaling, inflammatory response, complement, and coagulation (S9B Fig). Using GSEA
8 to capture dynamic changes in monocyte/macrophage functionality, we incorporated
9 Hallmark and KEGG terms and compared gene sets at baseline to gene sets at 7, 21,
10 and 28-dpi for each animal (S9C Fig). Considering the substantial influx of monocytes
11 with a less activated phenotype in the more immunocompromised animal (NV18) (Figs
12 9C and S8A-B), it was not surprising that GSEA comparing post-infection to baseline
13 revealed decreased enrichment in the majority of pathways examined (S9C Fig). NV18
14 also exhibited a decrease in the frequency of CD169 $+$ monocytes/macrophages on days
15 7 and 21 post-infection, further illustrating the limited functionality of the infiltrating
16 monocytes in this animal. In contrast, NV19 followed a more typical pattern with DEGs
17 enriched in the inflammatory response, cytokine and chemokine signaling, phagocytosis,
18 and proliferation at 7-dpi. Though we found no evidence of actively replicating virus at
19 the time, GSEA of days 21 and 28 post-infection revealed a continued enrichment of
20 pathways associated with the inflammatory response in NV19.

21

22 T cell Dynamics in Coinfected Animals

23 We also examined the T cell dynamics and phenotypes in the coinfecting animals (Fig
24 10). Using subclustering analysis, we identified five distinct T cell subclusters, each with
25 unique phenotypic characteristics. Populations 0, 2, and 3 had elevated expression of

1 *CD69* and *ITGAE* (CD103) (Fig 10D), indicative of a tissue-resident phenotype (T_{RM}).
2 Cluster 0 displayed a more cytotoxic phenotype, characterized by elevated expression of
3 *KLRD1*, *GZMB*, and *GZMK* (Fig 10C). Cluster 3 demonstrated an inflammatory
4 phenotype, with greater expression of *IFN- γ* and tumor necrosis factor (TNF) cytokines
5 *TNF* and *TNFSF8*, while cluster 2 represented an intermediate phenotype (Fig 10C).
6 Additionally, we identified infiltrating T cells (cluster 1) and proliferating T cells (cluster 4,
7 *MKI67^{hi}* and *HMGB2^{hi}*) (Fig 10D).

8

9 Coinciding with the substantial influx of less activated monocytes at 7 dpi, the more
10 immunocompromised animal, NV18, also experienced a notable shift in T cells towards
11 a more inert phenotype (cluster 1). This population dominated the T cell landscape and
12 persisted as the major population throughout the 28-day post-infection period (Fig 10B).
13 Moreover, NV18 displayed increases in the proportion of proliferating T cells (cluster 4)
14 at 7 and 21-dpi, indicating active cellular proliferation, accompanied by a substantial
15 decrease in the proportions of all three T_{RM} clusters. Our flow cytometry results indicated
16 that NV18 had a reduction in pulmonary CD3+ T cells following SARS-CoV-2 exposure.
17 Thus, the T cell patterns observed in our scRNAseq analysis for this animal most likely
18 reflect the preservation of specific subpopulations rather than actual increases. In
19 contrast, at 7-dpi, NV19 displayed an increase in the proportion of infiltrating T cells
20 (cluster 1) and a reciprocal decrease in T_{RM} cluster 0, although to a lesser extent than
21 the more immunocompromised animal (NV18). Notably, all other T cell populations
22 remained fairly stable in NV19.

23

24 **Discussion:**

1 Since its emergence in December 2019 in Wuhan, China, the novel coronavirus SARS-
2 CoV-2 has had a profound global impact [1]. COVID-19, caused by SARS-CoV-2,
3 encompasses a spectrum of disease manifestations, ranging from asymptomatic [50,51]
4 to mild flu-like symptoms to pneumonia [52,53]. While the majority of infected individuals
5 exhibit mild to moderate symptoms, a select group can experience severe complications
6 marked by significantly elevated levels of coagulation biomarkers and proinflammatory
7 cytokines, which can lead to acute respiratory distress syndrome (ARDS), and in some
8 cases, death [54]. Risk factors such as a compromised immune system, advanced age,
9 and comorbidities such as cardiovascular disease, diabetes, and obesity increase the
10 likelihood of severe disease.

11

12 The presence of HIV infection poses additional risks for individuals, including a
13 compromised immune system and a higher prevalence of cardiovascular disease,
14 raising concerns about the impact of HIV on the severity and persistence of SARS-CoV-
15 2 infections [13–15]. While initial research indicated similar or improved outcomes for
16 people living with HIV (PLWH) compared to the general population [16–18], larger
17 population-based studies reported higher rates of hospitalization and COVID-19-related
18 deaths among PLWH [19–23]. Recent studies suggest that unsuppressed viral loads or
19 low CD4+ T cell counts are associated with suboptimal cellular and humoral immune
20 responses to SARS-CoV-2 [24,25].

21

22 Immunodeficiency associated with HIV not only raises concerns about increased
23 severity but also the potential facilitation of SARS-CoV-2 persistence and evolution,
24 leading to the emergence of novel viral variants. Karim et al, (2021) highlighted this

1 concern in a recent study in which an individual with advanced HIV showed prolonged
2 shedding of SARS-CoV-2, high viral loads, and the development of multiple viral
3 mutations [26]. Although retrospective studies have explored the impact of HIV status on
4 COVID-19 incidence and severity, controlled studies in this area are lacking.

5

6 To address these gaps, we conducted a small pilot study involving two pigtail macaques
7 (PTMs) infected with SIVmac239, a strain that is highly pathogenic in PTM and models
8 progressive HIV infection, and subsequently exposed them to SARS-CoV-2 after
9 approximately one year. Notably, PTMs infected with SIV exhibit more rapid progression
10 to AIDS as compared to rhesus macaques and demonstrate cardiovascular
11 abnormalities similar to those observed in humans with advanced HIV, making them an
12 ideal model for evaluating the effects of chronic SIV infection on SARS-CoV-2 dynamics
13 [55–58]. Our study aimed to investigate the impact of SIV-induced immunodeficiency on
14 the clinical manifestation of COVID-19, along with its impacts on viral replication and
15 evolution in a controlled setting. We compared the clinical, virological, and
16 immunological outcomes of the coinfecting animals with our previously published cohort
17 of SIV-naïve PTMs infected with SARS-CoV-2 [27].

18

19 One of the key findings of our study is that SIV-induced immunodeficiency did not lead to
20 enhanced COVID-19 disease in the coinfecting animals. Despite the presence of
21 significant immunodeficiency, as evidenced by the severe reduction in CD4+ T cells, the
22 coinfecting animals exhibited only mild COVID-19 symptoms, similar to the control group.
23 This finding contrasts with previous studies that have reported a higher risk of severe
24 disease and mortality in PLWH [19–23], suggesting that aspects beyond

1 immunodeficiency, such as comorbidities or host-related factors, may contribute to the
2 elevated risk of severe COVID-19 observed in PLWH.

3

4 Our analysis of SARS-CoV-2 viral dynamics in the coinfecting animals revealed that SIV-
5 induced immunodeficiency did not significantly impact viral replication or evolution, with
6 viral dynamics indistinguishable from the controls. Despite higher levels of vRNA in
7 bronchoalveolar lavage (BAL) of the more immunocompromised animal (NV18), vRNA
8 levels became undetectable in both of the coinfecting animals by three- or four-weeks
9 post-infection in all sampled mucosal sites indicating that underlying SIV infection alone
10 is insufficient to drive uncontrolled SARS-CoV-2 replication.

11

12 However, we did observe a notable difference in the adaptive immune response to
13 SARS-CoV-2 infection between the SIV+ and SIV-naïve PTMs. By 21-dpi, the control
14 animals exhibited detectable SARS-CoV-2-specific neutralizing antibodies, IgA and IgG
15 binding antibodies, and virus-specific T cell responses. In contrast, both coinfecting
16 animals failed to generate virus-specific humoral or cellular immune responses against
17 SARS-CoV-2. This finding is consistent with studies linking uncontrolled HIV infection to
18 suboptimal T cell and antibody responses to SARS-CoV-2 [24,25]. These results
19 underscore the impact of pre-existing immunodeficiency on the development of adaptive
20 immunity during coinfection. The observed inability to mount effective virus-specific
21 cellular and humoral immune responses sheds light on the potential challenges faced by
22 individuals with advanced HIV infection when encountering SARS-CoV-2 and raises
23 concerns about the potential impacts of reinfection.

24

1 Additionally, we noted an influx of pulmonary infiltrating monocytes, which dominated the
2 immunological landscape in the coinfecting animals, compared to T cells in SIV-naïve
3 animals, as reported in our previous study. Our scRNAseq analysis provided additional
4 insights into nuances of the immune response in the coinfecting PTMs, particularly in the
5 more immunocompromised animal (NV18), which exhibited an influx of pulmonary
6 monocytes and T cells with diminished functionality. Immune dynamics in the less
7 immunocompromised animal (NV19) suggested a more balanced immune response.
8 The observed differences in pulmonary infiltrating immune cells between the two
9 coinfecting animals may be attributed to the varying levels of viremia, overall immune
10 competence, or subclinical pneumocystis infection in the more immunocompromised
11 animal (NV18).

12

13 **Conclusion:**

14 Overall, our study provides valuable insights into the interplay between SIV-induced
15 immunodeficiency and SARS-CoV-2 infection. Despite the notable immunodeficiency
16 observed in the coinfecting animals, we found no evidence of enhanced COVID-19
17 disease nor significant impacts on viral replication or evolution. However, the impaired T-
18 cell response and lack of neutralizing antibodies in the coinfecting animals highlight the
19 impact of underlying SIV-induced immunodeficiency on the immune response to SARS-
20 CoV-2. These findings contribute to our understanding of COVID-19 pathogenesis in
21 immunocompromised individuals and may help guide the development of strategies to
22 manage COVID-19 in vulnerable populations.

23

24 **Limitations:**

1 As this was a preliminary study involving only two animals, it will be necessary to
2 conduct follow-up studies with larger cohorts in order to validate our findings.
3 Nonetheless, our data provide novel important discoveries contributing to the growing
4 collection of SARS-CoV-2 resources. Further investigations into SARS-CoV-2 reinfection
5 of SIV+ nonhuman primates could serve as a promising follow-up to this study. Our
6 coinfection model demonstrated that the innate immune response-was likely efficient in
7 eliminating SARS-CoV-2 infection. A study that compares reinfection rates and viral
8 clearance upon secondary exposure would be an exciting next avenue to pursue.

9

10 **Acknowledgements:**

11 Work described in this report was conducted at the Tulane National Primate Research
12 Center (RRID: SCR_008167) with support from TNPRC core labs (RRIDs: SCR_024606,
13 SCR_024609, SCR_024613, SCR_024611, SCR_024612, SCR_024614, SCR_024610,
14 SCR_024679). Pigtail macaques were purpose bred at the Johns Hopkins University
15 breeding colony supported by U42OD013111. Work was supported by instrumentation
16 support funds NIH S10 OD026800 and NIH S10 OD030347. The following reagent was
17 obtained from BEI Resources; SARS-CoV-2 isolate WA1/2020 (NR-52281). We thank
18 Kejing Song for help with sequencing, and Ann-Marie May and Carli Thompson from the
19 Tulane Office of Biosafety for oversight of experiments in BSL-3 containment.

20

21 **Funding:**

22 This work was supported by NIH grants P51OD011104 (the TNPRC base grant) and
23 R01 AI138782 (JAH and NJM). The funders had no role in study design or decision to

1 publish.

2

3

4 **References:**

5 1. Organization WH. WHO COVID-19 Dashboard. World Health Organisation. 2023.

6 Available: <https://covid19.who.int>

7 2. Sayampanathan AA, Heng CS, Pin PH, Pang J, Leong TY, Lee VJ. Infectivity of
8 asymptomatic versus symptomatic COVID-19. Lancet. 2021;397: 93–94.

9 doi:10.1016/S0140-6736(20)32651-9

10 3. Teo AKJ, Choudhury Y, Tan IB, Cher CY, Chew SH, Wan ZY, et al. Saliva is more
11 sensitive than nasopharyngeal or nasal swabs for diagnosis of asymptomatic and
12 mild COVID-19 infection. Sci Rep. 2021;11: 1–8. doi:10.1038/s41598-021-82787-
13 z

14 4. Xie C, Li Q, Li L, Peng X, Ling Z, Xiao B, et al. Association of early inflammation
15 with age and asymptomatic disease in covid-19. J Inflamm Res. 2021;14: 1207–
16 1216. doi:10.2147/JIR.S304190

17 5. Zhu J, Ji P, Pang J, Zhong Z, Li H, He C, et al. Clinical characteristics of 3062
18 COVID-19 patients: A meta-analysis. J Med Virol. 2020;92: 1902–1914.
19 doi:10.1002/jmv.25884

20 6. McElvaney OJ, McEvoy NL, McElvaney OF, Carroll TP, Murphy MP, Dunlea DM,
21 et al. Characterization of the inflammatory response to severe COVID-19 illness.
22 Am J Respir Crit Care Med. 2020;202: 812–821. doi:10.1164/rccm.202005-
23 1583OC

1 7. Zhang R, Liu Y, Zhang B, Wu C, Zhou J, Zhang Y, et al. Coagulopathy is
2 associated with multiple organ damage and prognosis of COVID-19. EXCLI J.
3 2021;20: 174–191. doi:10.17179/excli2020-2853

4 8. Gao Y dong, Ding M, Dong X, Zhang J jin, Kursat Azkur A, Azkur D, et al. Risk
5 factors for severe and critically ill COVID-19 patients: A review. Allergy Eur J
6 Allergy Clin Immunol. 2021;76: 428–455. doi:10.1111/all.14657

7 9. Zhou Y, Chi J, Lv W, Wang Y. Obesity and diabetes as high-risk factors for severe
8 coronavirus disease 2019 (Covid-19). Diabetes Metab Res Rev. 2021;37: e3377.
9 doi:10.1002/dmrr.3377

10 10. Murray JF, Felton CP, Garay SM, Gottlieb MS, Hopewell PC, Stover DE, et al.
11 Pulmonary complications of the acquired immunodeficiency syndrome. Report of
12 a National Heart, Lung, and Blood Institute workshop. N Engl J Med. 1984;310:
13 1682–1688. doi:10.1056/NEJM198406213102529

14 11. Peters SG, Prakash UB. Pneumocystis carinii pneumonia. Review of 53 cases.
15 Am J Med. 1987;82: 73–78. doi:10.1016/0002-9343(87)90380-9

16 12. Stringer JR, Walzer PD. Molecular biology and epidemiology of Pneumocystis
17 carinii infection in AIDS. AIDS (London, England). England; 1996. pp. 561–571.
18 doi:10.1097/00002030-199606000-00001

19 13. Altuntas Aydin O, Kumbasar Karaosmanoglu H, Kart Yasar K. HIV/SARS-CoV-2
20 coinfected patients in Istanbul, Turkey. Journal of Medical Virology. John Wiley
21 and Sons Inc; 2020. pp. 2288–2290. doi:10.1002/jmv.25955

22 14. Hattab S, Guiguet M, Carcelain G, Fourati S, Guihot A, Autran B, et al. Soluble
23 biomarkers of immune activation and inflammation in HIV infection: Impact of 2

1 years of effective first-line combination antiretroviral therapy. *HIV Med.* 2015;16:
2 553–562. doi:10.1111/hiv.12257

3 15. Abbasi SAA, Noor T, Mylavaramu M, Sahotra M, Bashir HA, Bhat RR, et al.
4 Double Trouble Co-Infections: Understanding the Correlation Between COVID-19
5 and HIV Viruses. *Cureus.* 2023. doi:10.7759/cureus.38678

6 16. Guo W, Ming F, Dong Y, Zhang Q, Liu L, Gao M, et al. Driving force of COVID-19
7 among people living with HIV in Wuhan, China. *AIDS Care.* 2022;34: 1364–1371.
8 doi:10.1080/09540121.2022.2052259

9 17. Calza L, Bon I, Tadolini M, Borderi M, Colangeli V, Badia L, et al. COVID-19 in
10 patients with HIV-1 infection: a single-centre experience in northern Italy.
11 *Infection.* 2021;49: 333–337. doi:10.1007/s15010-020-01492-7

12 18. Lee KW, Yap SF, Ngeow YF, Lye MS. COVID-19 in People Living with HIV: A
13 Systematic Review and Meta-Analysis. *International Journal of Environmental
14 Research and Public Health.* 2021. doi:10.3390/ijerph18073554

15 19. Prabhu S, Poongulali S, Kumarasamy N. Impact of COVID-19 on people living
16 with HIV: A review. *J Virus Erad.* 2020;6: 100019. doi:10.1016/j.jve.2020.100019

17 20. Geretti AM, Stockdale AJ, Kelly SH, Cevik M, Collins S, Waters L, et al. Outcomes
18 of Coronavirus Disease 2019 (COVID-19) Related Hospitalization Among People
19 With Human Immunodeficiency Virus (HIV) in the ISARIC World Health
20 Organization (WHO) Clinical Characterization Protocol (UK): A Prospective
21 Observational Study. *Clin Infect Dis.* 2021;73: e2095–e2106.
22 doi:10.1093/cid/ciaa1605

23 21. Bhaskaran K, Rentsch CT, MacKenna B, Schultze A, Mehrkar A, Bates CJ, et al.

1 HIV infection and COVID-19 death: a population-based cohort analysis of UK
2 primary care data and linked national death registrations within the OpenSAFELY
3 platform. *Lancet HIV*. 2021;8: e24–e32. doi:10.1016/S2352-3018(20)30305-2

4 22. Tesoriero JM, Swain CAE, Pierce JL, Zamboni L, Wu M, Holtgrave DR, et al.
5 COVID-19 Outcomes among Persons Living with or without Diagnosed HIV
6 Infection in New York State. *JAMA Netw Open*. 2021;4: 1–14.
7 doi:10.1001/jamanetworkopen.2020.37069

8 23. Bertagnolio S, Thwin SS, Silva R, Nagarajan S, Jassat W, Fowler R, et al. Clinical
9 features of, and risk factors for, severe or fatal COVID-19 among people living
10 with HIV admitted to hospital: analysis of data from the WHO Global Clinical
11 Platform of COVID-19. *Lancet HIV*. 2022;9: e486–e495. doi:10.1016/S2352-
12 3018(22)00097-2

13 24. Nkosi T, Chasara C, Papadopoulos AO, Nguni TL, Karim F, Moosa MYS, et al.
14 Unsuppressed HIV infection impairs T cell responses to SARS-CoV-2 infection
15 and abrogates T cell cross-recognition. *Elife*. 2022;11. doi:10.7554/ELIFE.78374

16 25. Riou C, du Bruyn E, Stek C, Daroowala R, Goliath RT, Abrahams F, et al.
17 Relationship of SARS-CoV-2-specific CD4 response to COVID-19 severity and
18 impact of HIV-1 and tuberculosis coinfection. *J Clin Invest*. 2021;131: 1–15.
19 doi:10.1172/JCI149125

20 26. Karim F, Moosa MYS, Gosnell BI, Cele S, Giandhari J, Pillay S, et al. Persistent
21 SARS-CoV-2 infection and intra-host evolution in association with advanced HIV
22 infection. *medRxiv*. 2021; 2021.06.03.21258228.
23 doi:10.1101/2021.06.03.21258228

24 27. Melton A, Doyle-Meyers LA, Blair R V., Midkiff C, Melton HJ, Russell-Lodrigue K,

1 et al. The pigtail macaque (*Macaca nemestrina*) model of COVID-19 reproduces
2 diverse clinical outcomes and reveals new and complex signatures of disease.
3 PLOS Pathogens. 2021. doi:10.1371/journal.ppat.1010162

4 28. Li H, Wang S, Kong R, Ding W, Lee F-H, Parker Z, et al. Envelope residue 375
5 substitutions in simian-human immunodeficiency viruses enhance CD4 binding
6 and replication in rhesus macaques. Proc Natl Acad Sci U S A. 2016;113: E3413-
7 22. doi:10.1073/pnas.1606636113

8 29. Beddingfield BJ, Maness NJ, Fears AC, Rappaport J, Aye PP, Russell-Lodrigue
9 K, et al. Effective Prophylaxis of COVID-19 in Rhesus Macaques Using a
10 Combination of Two Parenterally-Administered SARS-CoV-2 Neutralizing
11 Antibodies. Front Cell Infect Microbiol. 2021;11: 753444.
12 doi:10.3389/fcimb.2021.753444

13 30. Amanat F, White KM, Miorin L, Strohmeier S, McMahon M, Meade P, et al. An In
14 Vitro Microneutralization Assay for SARS-CoV-2 Serology and Drug Screening.
15 Curr Protoc Microbiol. 2020;58: 1–15. doi:10.1002/cpmc.108

16 31. Butler A, Hoffman P, Smibert P, Papalexi E, Satija R. Integrating single-cell
17 transcriptomic data across different conditions, technologies, and species. Nat
18 Biotechnol. 2018;36: 411–420. doi:10.1038/nbt.4096

19 32. Korsunsky I, Millard N, Fan J, Slowikowski K, Zhang F, Wei K, et al. Fast,
20 sensitive and accurate integration of single-cell data with Harmony. Nat Methods.
21 2019;16: 1289–1296. doi:10.1038/s41592-019-0619-0

22 33. Zhou Y, Zhou B, Pache L, Chang M, Khodabakhshi AH, Tanaseichuk O, et al.
23 Metascape provides a biologist-oriented resource for the analysis of systems-level
24 datasets. Nat Commun. 2019;10: 1523. doi:10.1038/s41467-019-09234-6

1 34. Liberzon A, Birger C, Thorvaldsdóttir H, Ghandi M, Mesirov JP, Tamayo P. The
2 Molecular Signatures Database Hallmark Gene Set Collection. *Cell Syst.* 2015;1:
3 417–425. doi:10.1016/j.cels.2015.12.004

4 35. Subramanian A, Tamayo P, Mootha VK, Mukherjee S, Ebert BL, Gillette MA, et al.
5 Gene set enrichment analysis: A knowledge-based approach for interpreting
6 genome-wide expression profiles. *Proc Natl Acad Sci.* 2005;102: 15545–15550.
7 doi:10.1073/pnas.0506580102

8 36. Liberzon A, Subramanian A, Pinchback R, Thorvaldsdóttir H, Tamayo P, Mesirov
9 JP. Molecular signatures database (MSigDB) 3.0. *Bioinformatics.* 2011;27: 1739–
10 1740. doi:10.1093/bioinformatics/btr260

11 37. Korotkevich G, Sukhov V, Budin N, Shpak B, Artyomov MN, Sergushichev A. Fast
12 gene set enrichment analysis. *bioRxiv.* 2021; 60012. doi:10.1101/060012

13 38. Kanehisa M, Goto S. KEGG: kyoto encyclopedia of genes and genomes. *Nucleic
14 Acids Res.* 2000;28: 27–30. doi:10.1093/nar/28.1.27

15 39. Kanehisa M. Toward understanding the origin and evolution of cellular organisms.
16 *Protein Sci.* 2019;28: 1947–1951. doi:10.1002/pro.3715

17 40. Kanehisa M, Furumichi M, Sato Y, Kawashima M, Ishiguro-Watanabe M. KEGG
18 for taxonomy-based analysis of pathways and genomes. *Nucleic Acids Res.*
19 2023;51: D587–D592. doi:10.1093/nar/gkac963

20 41. Huang C, Wang Y, Li X, Ren L, Zhao J, Hu Y, et al. Clinical features of patients
21 infected with 2019 novel coronavirus in Wuhan, China. *Lancet.* 2020;395: 497–
22 506. doi:10.1016/S0140-6736(20)30183-5

23 42. Bösmüller H, Matter M, Fend F, Tzankov A. The pulmonary pathology of COVID-

1 19. *Virchows Arch.* 2021/02/19. 2021;478: 137–150. doi:10.1007/s00428-021-03053-1

2

3 43. Fahlberg MD, Blair R V., Doyle-Meyers LA, Midkiff CC, Zenere G, Russell-
4 Lodrigue KE, et al. Cellular events of acute, resolving or progressive COVID-19 in
5 SARS-CoV-2 infected non-human primates. *Nat Commun.* 2020;11: 1–14.
6 doi:10.1038/s41467-020-19967-4

7 44. Blair R V, Vaccari M, Doyle-Meyers LA, Roy CJ, Russell-Lodrigue K, Fahlberg M,
8 et al. Acute Respiratory Distress in Aged, SARS-CoV-2-Infected African Green
9 Monkeys but Not Rhesus Macaques. *Am J Pathol.* 2021;191: 274–282.
10 doi:10.1016/j.ajpath.2020.10.016

11 45. Qin C, Zhou L, Hu Z, Zhang S, Yang S, Tao Y, et al. Dysregulation of Immune
12 Response in Patients With Coronavirus 2019 (COVID-19) in Wuhan, China. *Clin
13 Infect Dis* [an Off Publ Infect Dis Soc Am]. 2020;71: 762–768.
14 doi:10.1093/cid/ciaa248

15 46. Wang D, Hu B, Hu C, Zhu F, Liu X, Zhang J, et al. Clinical Characteristics of 138
16 Hospitalized Patients With 2019 Novel Coronavirus-Infected Pneumonia in
17 Wuhan, China. *JAMA.* 2020;323: 1061–1069. doi:10.1001/jama.2020.1585

18 47. Speranza E, Williamson BN, Feldmann F, Sturdevant GL, Pérez-Pérez L, Meade-
19 White K, et al. Single-cell RNA sequencing reveals SARS-CoV-2 infection
20 dynamics in lungs of African green monkeys. *Sci Transl Med.* 2021;13.
21 doi:10.1126/scitranslmed.abe8146

22 48. Lee JS, Koh JY, Yi K, Kim Y II, Park SJ, Kim EH, et al. Single-cell transcriptome of
23 bronchoalveolar lavage fluid reveals sequential change of macrophages during
24 SARS-CoV-2 infection in ferrets. *Nat Commun.* 2021;12. doi:10.1038/s41467-021-

1 24807-0

2 49. Baitsch D, Bock HH, Engel T, Telgmann R, Müller-Tidow C, Varga G, et al.

3 Apolipoprotein e induces antiinflammatory phenotype in macrophages.

4 Arterioscler Thromb Vasc Biol. 2011;31: 1160–1168.

5 doi:10.1161/ATVBAHA.111.222745

6 50. Gandhi M, Yokoe DS, Havlir D V. Asymptomatic Transmission, the Achilles' Heel

7 of Current Strategies to Control Covid-19. N Engl J Med. 2020/04/24. 2020;382:

8 2158–2160. doi:10.1056/NEJMe2009758

9 51. Gatto M, Bertuzzo E, Mari L, Miccoli S, Carraro L, Casagrandi R, et al. Spread

10 and dynamics of the COVID-19 epidemic in Italy: Effects of emergency

11 containment measures. Proc Natl Acad Sci U S A. 2020/04/23. 2020;117: 10484–

12 10491. doi:10.1073/pnas.2004978117

13 52. Guan W-J, Ni Z-Y, Hu Y, Liang W-H, Ou C-Q, He J-X, et al. Clinical

14 Characteristics of Coronavirus Disease 2019 in China. N Engl J Med. 2020/02/28.

15 2020;382: 1708–1720. doi:10.1056/NEJMoa2002032

16 53. Kujawski SA, Wong KK, Collins JP, Epstein L, Killerby ME, Midgley CM, et al.

17 Clinical and virologic characteristics of the first 12 patients with coronavirus

18 disease 2019 (COVID-19) in the United States. Nat Med. 2020;26: 861–868.

19 doi:10.1038/s41591-020-0877-5

20 54. Wu JT, Leung K, Bushman M, Kishore N, Niehus R, de Salazar PM, et al.

21 Estimating clinical severity of COVID-19 from the transmission dynamics in

22 Wuhan, China. Nat Med. 2020/03/19. 2020;26: 506–510. doi:10.1038/s41591-

23 020-0822-7

1 55. Canary LA, Vinton CL, Morcock DR, Pierce JB, Estes JD, Brenchley JM, et al.
2 Rate of AIDS progression is associated with gastrointestinal dysfunction in simian
3 immunodeficiency virus-infected pigtail macaques. *J Immunol.* 2013/02/11.
4 2013;190: 2959–2965. doi:10.4049/jimmunol.1202319

5 56. Klatt NR, Canary LA, Vanderford TH, Vinton CL, Engram JC, Dunham RM, et al.
6 Dynamics of simian immunodeficiency virus SIVmac239 infection in pigtail
7 macaques. *J Virol.* 2011/11/16. 2012;86: 1203–1213. doi:10.1128/JVI.06033-11

8 57. Klatt NR, Harris LD, Vinton CL, Sung H, Briant JA, Tabb B, et al. Compromised
9 gastrointestinal integrity in pigtail macaques is associated with increased microbial
10 translocation, immune activation, and IL-17 production in the absence of SIV
11 infection. *Mucosal Immunol.* 2010/03/31. 2010;3: 387–398.
12 doi:10.1038/mi.2010.14

13 58. Metcalf Pate KA, Lyons CE, Dorsey JL, Shirk EN, Queen SE, Adams RJ, et al.
14 Platelet Activation and Platelet-Monocyte Aggregate Formation Contribute to
15 Decreased Platelet Count During Acute Simian Immunodeficiency Virus Infection
16 in Pig-tailed Macaques. *J Infect Dis.* 2013;208: 874–883. doi:10.1093/infdis/jit278

17

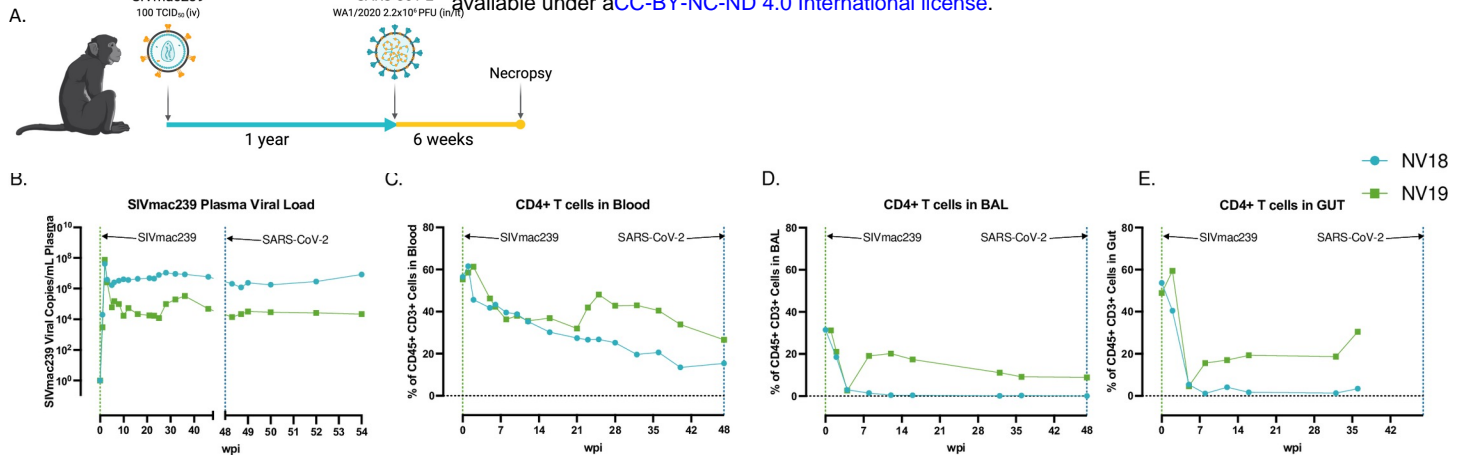


Figure 1. Before SARS-CoV-2 exposure, PTM experienced uncontrolled SIV viremia and immunodeficiency due to loss of CD4+ T cells. A. Overall study design. Two female pigtail macaques (PTM, NV18 & NV19) were inoculated with SIVmac239 (100 TCID₅₀, iv), followed by SARS-CoV-2 (Wa1/2020, 2x10⁶, in/it) challenge approximately one year later. Figure created with BioRender (<https://BioRender.com>). **B.** Quantification of SIVmac239 RNA levels in plasma overtime (Quantitative RT PCR). **C-E.** CD4+ T cell kinetics following SIVmac239 infection in blood (**C**), bronchoalveolar lavage (BAL) (**D**), and gut (**E**).

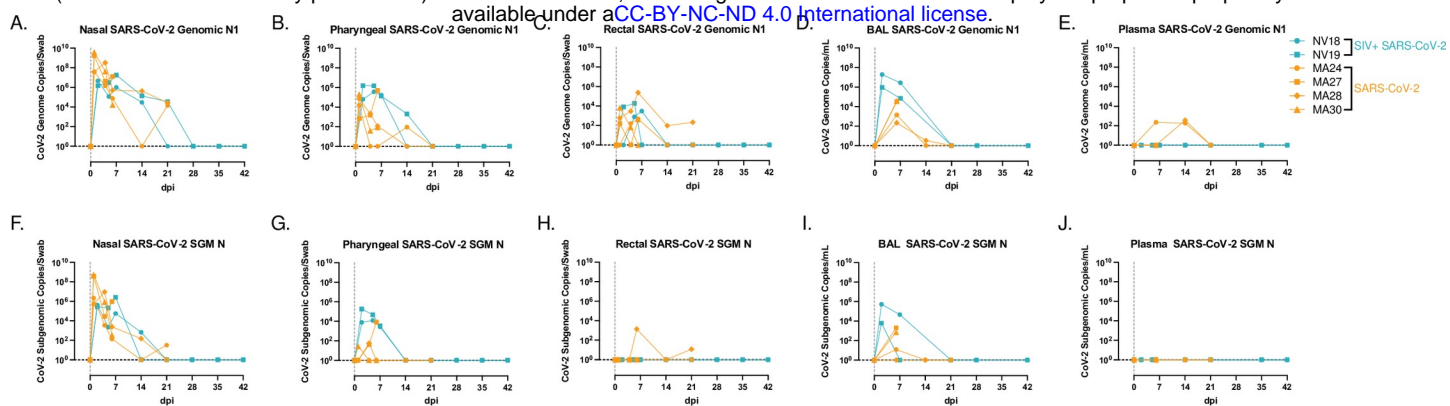


Figure 2. SARS-CoV-2 viral dynamics. NV18 and NV19 were inoculated with SARS-CoV-2 (1×10^6 TCID₅₀) 48 weeks post SIVmac239 infection through a combination of intranasal (in) and intratracheal (it) exposure, indicated as Day 0. **A-J.** Comparison of genomic (A-E) and subgenomic (SGM, F-J) SARS-CoV-2 mRNA levels in mucosal swabs (A-C, F-H), BAL supernatant (D, I) and plasma (E, J) in coinfecting animals (blue) and a previously published cohort of SIV naïve PTM (orange).

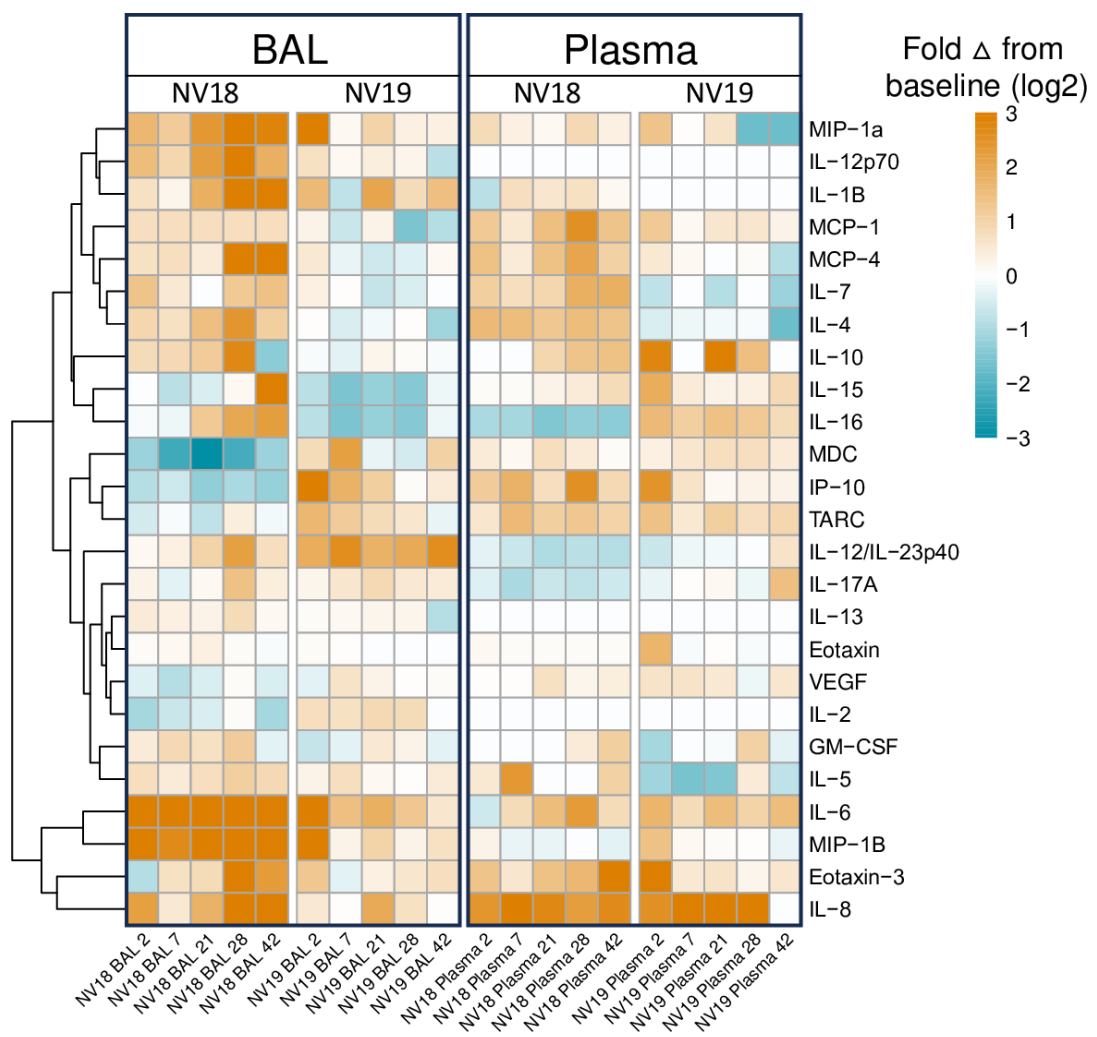


Figure 3. Meso Scale analysis of cytokine and chemokine fluctuations in blood and BAL in PTM coinfecting with SIV and SARS-CoV-2. A. Heatmap indicating changes in cytokine and chemokine levels in BAL supernatant and plasma. Data represents log₂ fold change from baseline (pre-SARS-CoV-2 infection). **B-YY.** Line graphs illustrating cytokine, proinflammatory cytokine, and chemokine dynamics in BAL supernatant (**B-H, P-W, FF-YY**) and plasma (**I-O, X-EE, PP-YY**) before and 2-, 7-, 21-, 28-, and 42-days post SARS-CoV-2 infection.

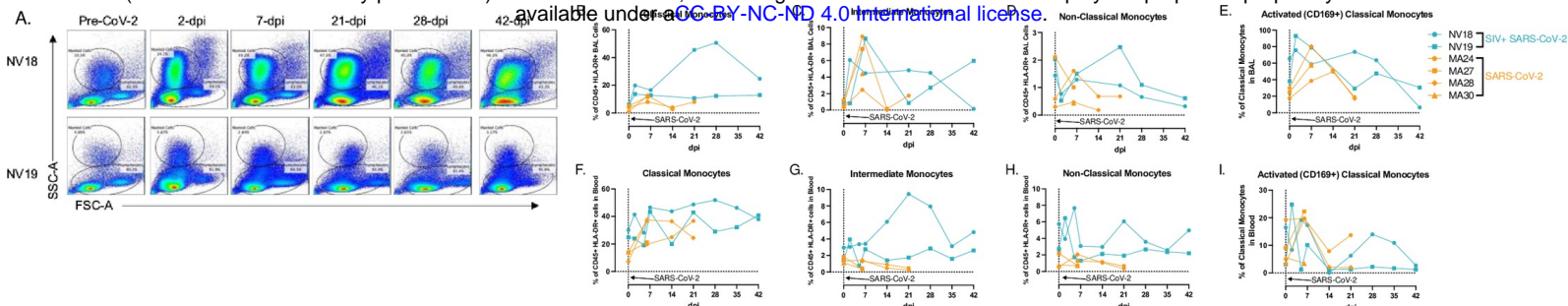
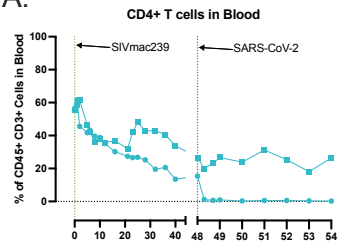
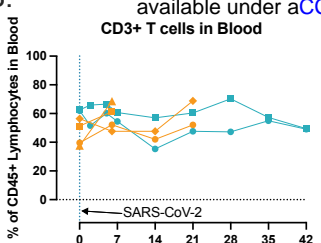


Figure 4. Monocyte/macrophage kinetics in BAL and blood following SARS-CoV-2 infection of SIV+ and SIV naïve PTM. **A.** Representative flow cytometry dot plots of pulmonary infiltrating myeloid cells and lymphocytes in the lungs of two SIV+ PTM before and 2, 7, 21, 28, and 42 days after SARS-CoV-2 exposure. Gated on Time>Live>Single cells>CD45+>SSC-A vs FSC-A. **B-E, F-I.** Frequencies of Classical (CD45+ HLA-DR+ CD14+ CD16-) (**B,F**) intermediate (CD45+ HLA-DR+ CD14+ CD16+) (**C,G**), and non-classical monocytes (CD45+ HLA-DR+ CD14- CD16+) (**D,H**) in BAL (**B-D**) and blood (**F-H**) before and after SARS-CoV-2 infection. Day 0 = day of SARS-CoV-2 infection. **E,I.** Activated Classical Monocytes (CD169+) in BAL and blood. Figures B-I: SIVmac239/SARS-CoV-2 infected PTM (blue), and SARS-CoV-2 only infected PTM (orange).

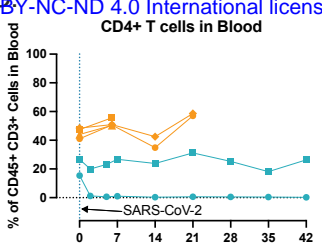
A.



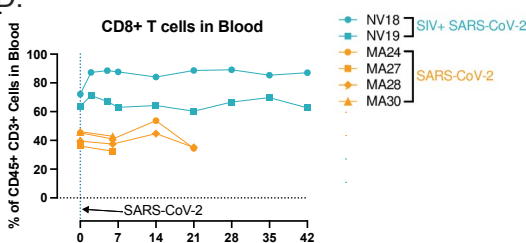
B.



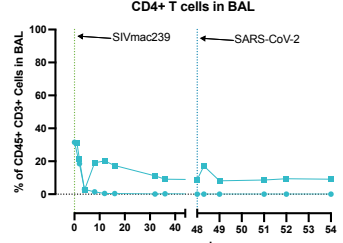
C. CD4+ T cells in Blood



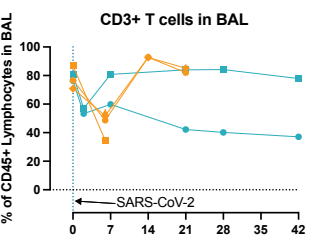
D.



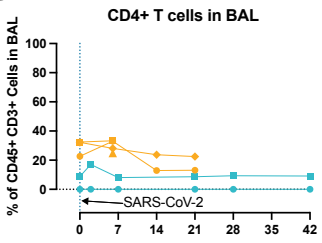
E.



F.



G.



H.

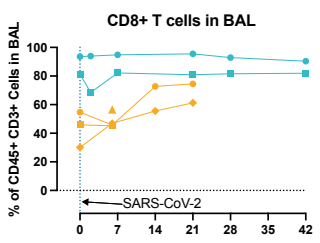
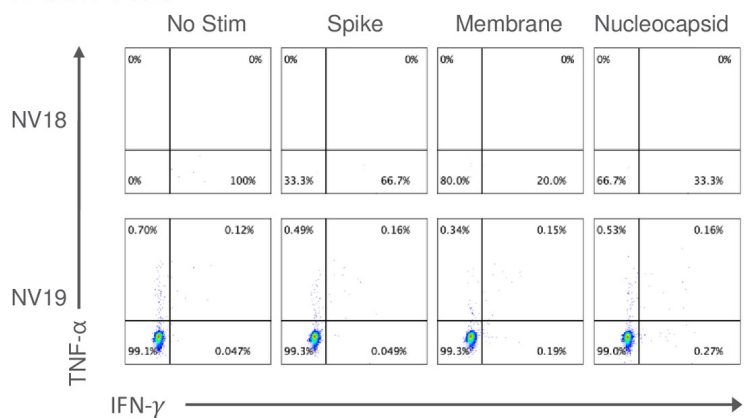


Figure 5. T cell dynamics in blood and BAL following SARS-CoV-2 infection of SIV+ and SIV naïve PTM. CD4+ T cell kinetics in blood (A) and BAL (G), following SIVmac239 and SARS-CoV-2 infection. H-L. Peripheral and pulmonary T cell dynamics in SIV+ SARS-CoV-2 coinfecting PTM (blue). Historical data from four SIV naïve SARS-CoV-2 infected PTM in orange. Comparison of overall CD3+ T cell populations (B&F) as well as T cell subsets; CD4+ (C&G), CD8+ (D&H).

A. CD4+ T cells



B. CD8+ T cells

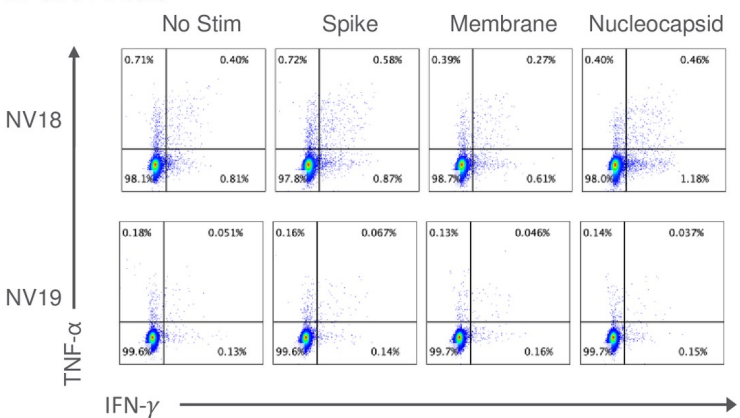


Figure 6. SARS-CoV-2 specific T cell responses were undetectable in the lung 21-days-post-infection. Two female pigtail macaques (PTM, NV18 & NV19) co-infected with SIVmac239 and SARS-CoV-2 shown. **A&B.** Flow cytometry dot plots demonstrating the IFN- γ and TNF- α response of CD4+ (**A**) and CD8+ (**B**) T cells to overnight SARS-CoV-2 peptide (spike, membrane, and nucleocapsid) stimulation. No Stim = cells incubated overnight without peptide stimulation.

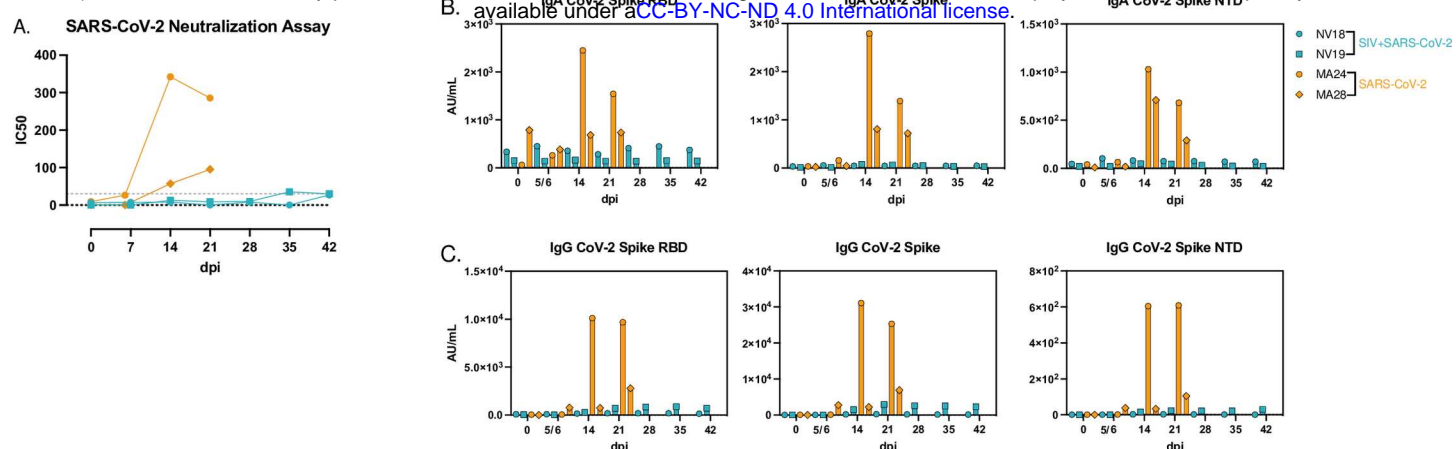


Figure 7. Humoral immune response to SARS-CoV-2 infection. A. SARS-CoV-2 neutralization assay depicting serum antibody levels against SARS-CoV-2 using Vero TMPRSS2 cells. **B&C.** MesoScale analysis of IgA (**B**) and IgG (**C**) binding antibodies to SARS-CoV-2 Spike receptor binding domain (RBD), Spike glycoprotein 1 and 2 (S1&S2), and Spike N-Terminal Domain (NTD).

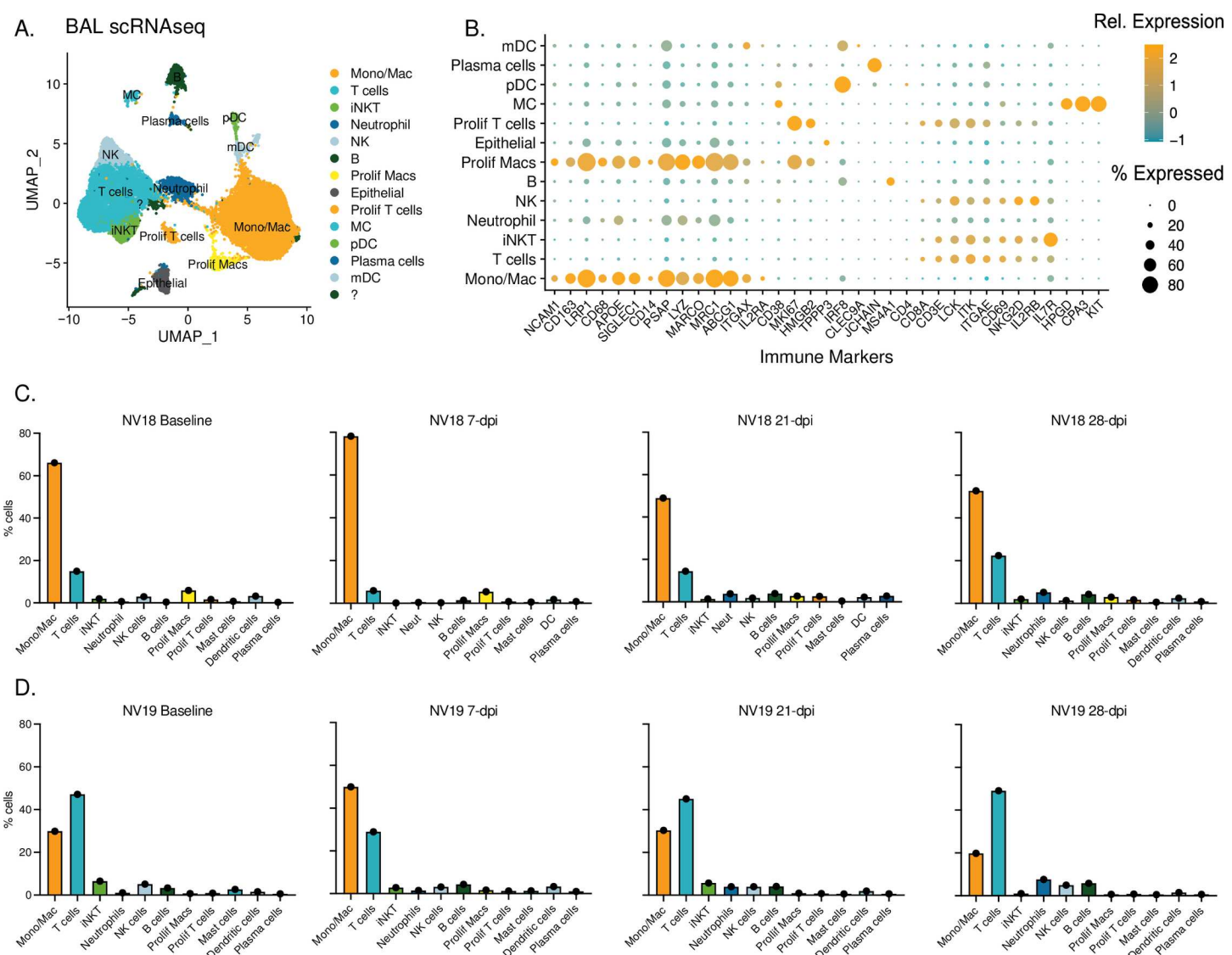
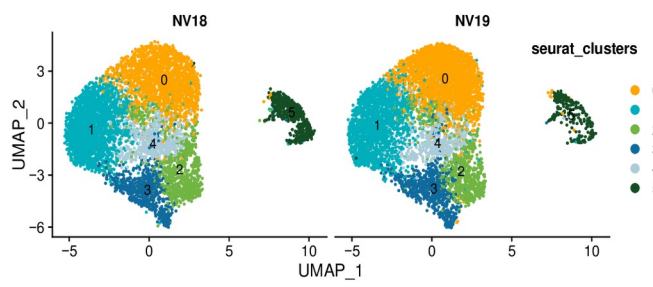


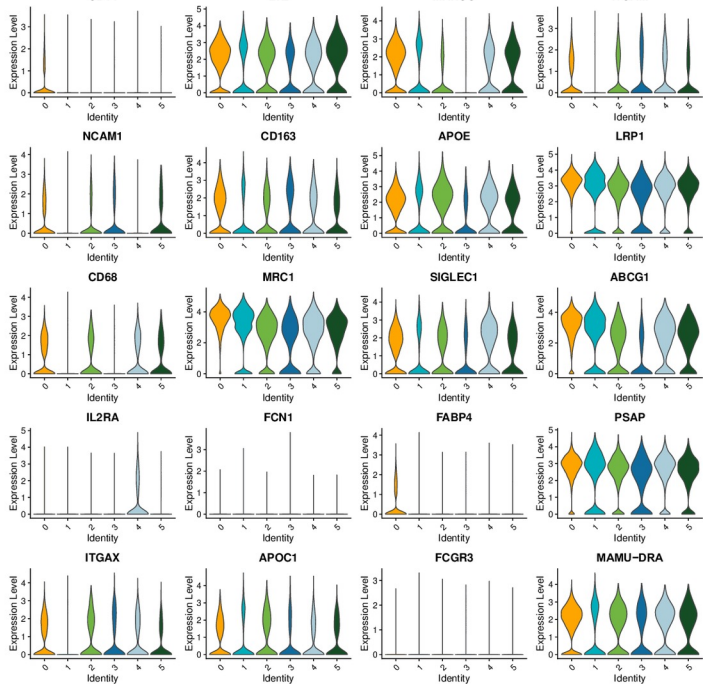
Figure 8. Single-cell classification and dynamics of bronchoalveolar lavage cell populations during SIV/SARS-CoV-2 coinfection. A. UMAP plots illustrating scRNAseq data obtained from BAL sampling of PTMs (NV18 and NV19) coinfecting with SIV and SARS-CoV-2. **B.** Gene markers utilized for cell type identification. Dot color represents relative gene expression (Rel. Expression), while dot size indicates the proportion of cells expressing the gene (% Expression). Refer to supplemental figure 6 for additional genes used. **C-D.** Immune cell dynamics in BAL during SARS-CoV-2 infection for the more immunocompromised animal, NV18, (**C**) and NV19 (**D**). The baseline (BL) sample was collected prior to SARS-CoV-2 exposure at 48 weeks post-SIV infection.

MC = Mast cells, pDC = plasmacytoid dendritic cells, mDC = myeloid dendritic cells, NK = natural killer cells

A. Subclustering of BAL Monocytes/Macrophages



B.



C.

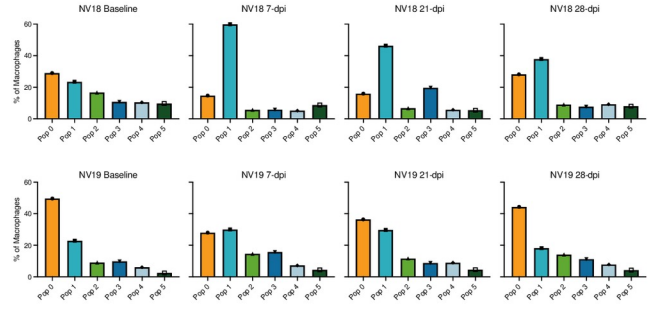


Figure 9. Monocyte/macrophage dynamics following SARS-CoV-2 inoculation of SIV+ PTM. A. UMAP plots of pulmonary monocyte/macrophage (mono/mac) subclustering. B. Violin Plots illustrating expression of canonical monocyte/macrophage gene signatures among the Seurat-derived clusters. C. Monocyte/macrophage dynamics during SARS-CoV-2 infection.

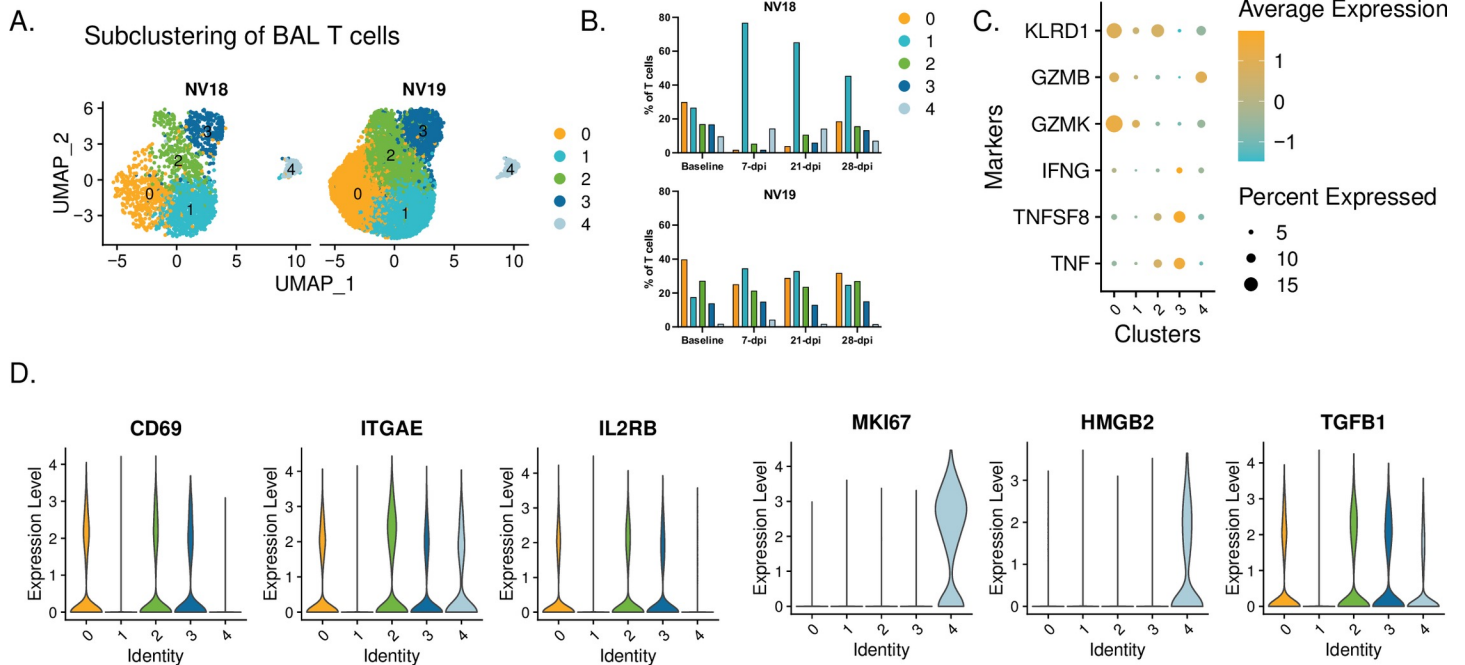
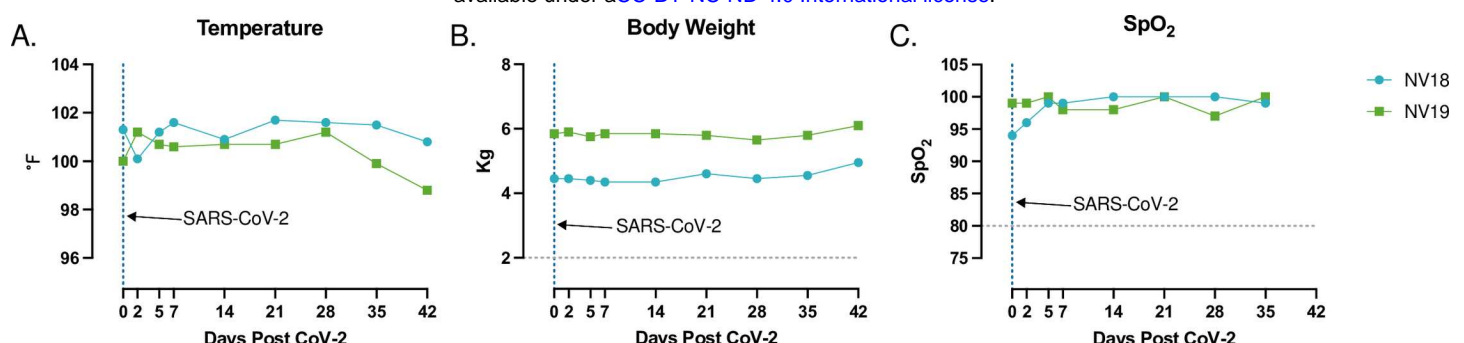
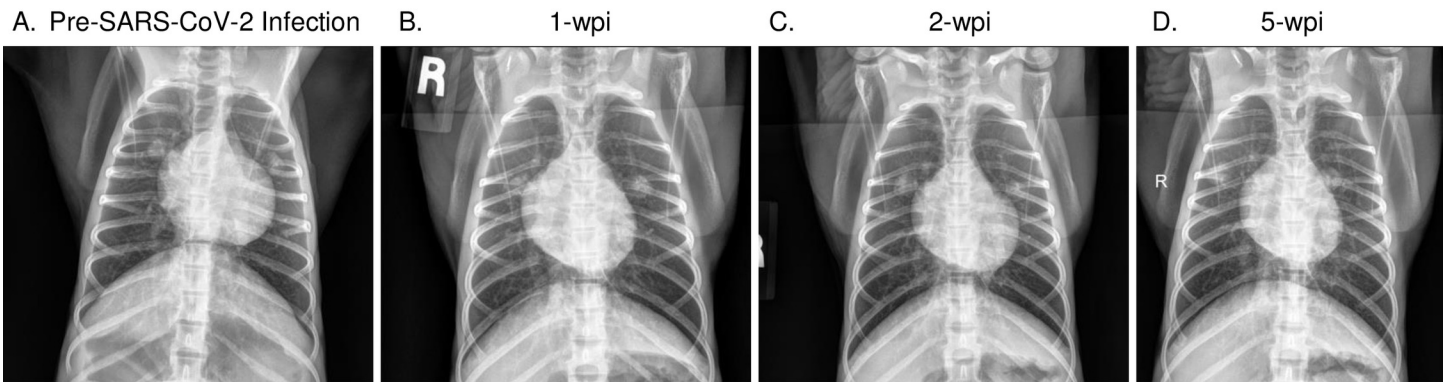


Figure 10. T cell dynamics. **A.** UMAP plots showing subclustered T cells. **B.** T cell dynamics during SARS-CoV-2 infection. **C.** Dot plot depicting proinflammatory cytokine and cytotoxic marker expression by cluster. **D.** Violin plots depicting gene expression of T cell markers in Seurat-derived T cell clusters.

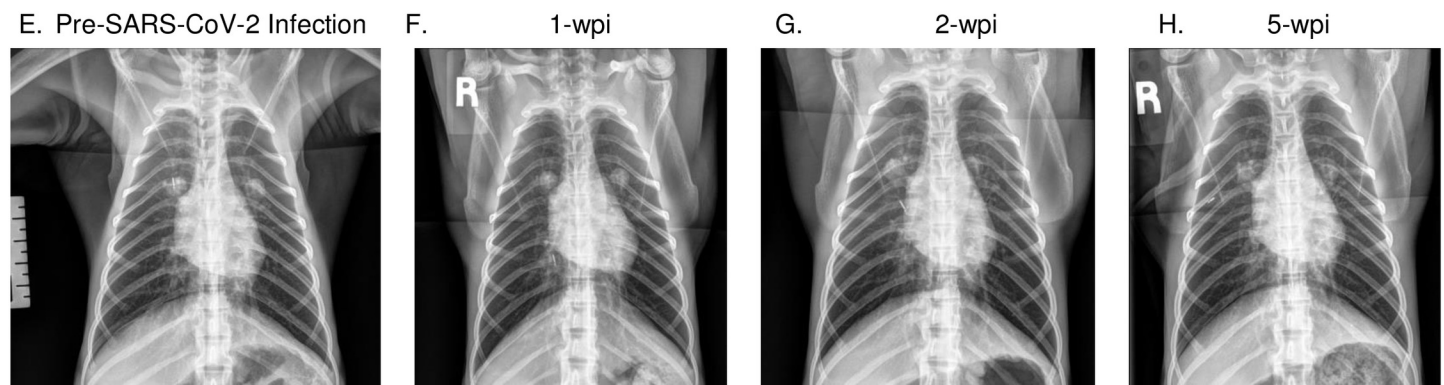


Supplemental Figure 1. Temperature (A), weight (B), and saturation of peripheral oxygen (SpO₂) (C) levels were measured prior to and for 6 weeks following SARS-CoV-2 inoculation of SIV+ pigtail macaques. Day 0 indicates time of SARS-CoV-2 infection, 48 weeks post SIVmac239 exposure.

NV18

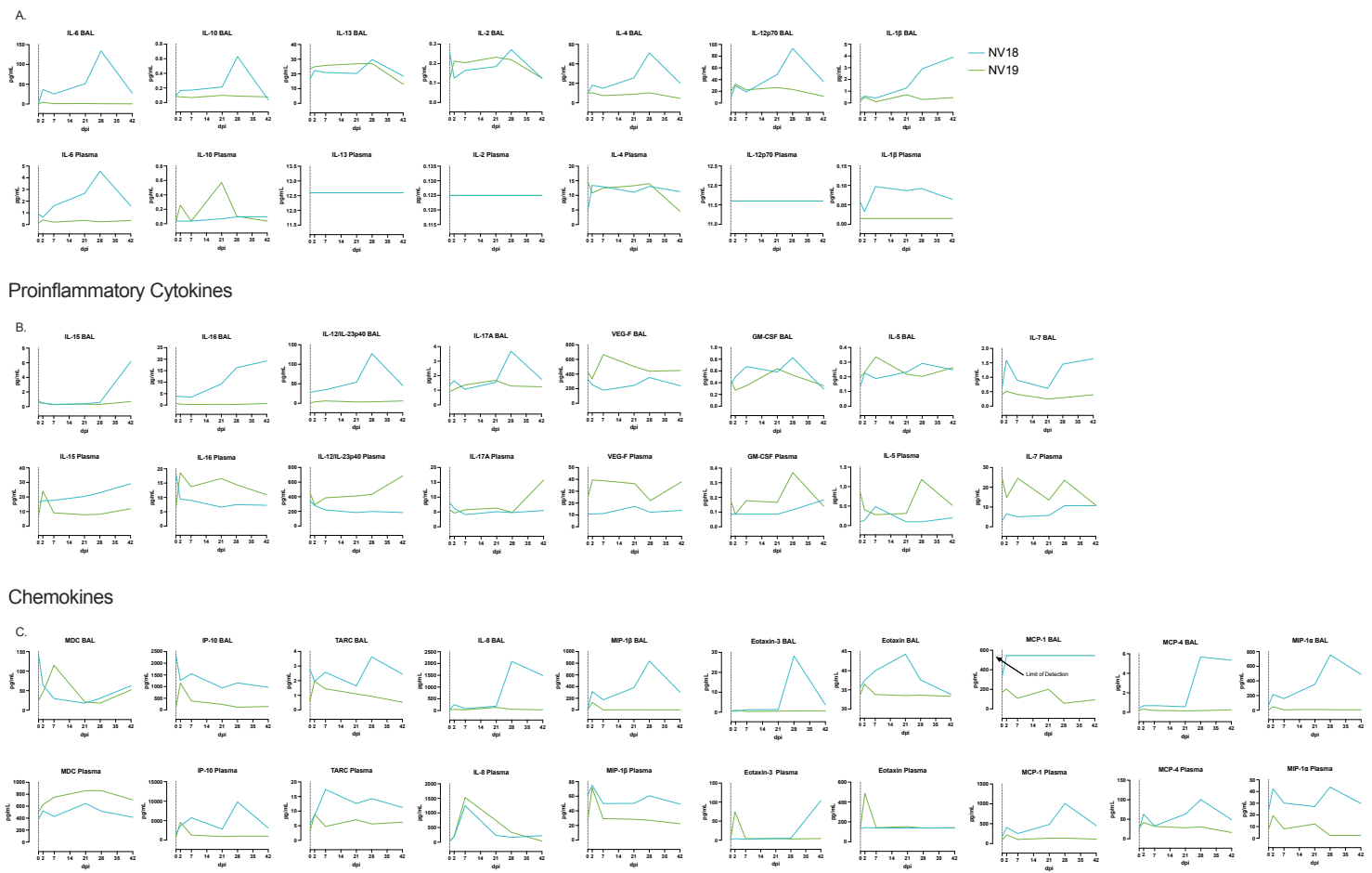


NV19



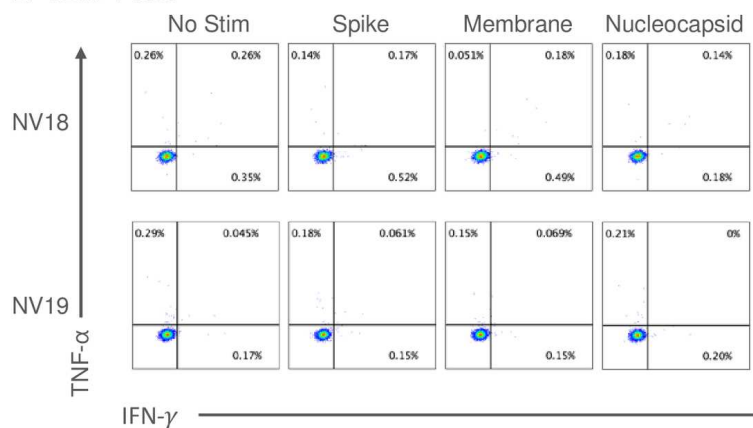
Supplemental Figure 2. Radiographs of SIV-infected pigtail macaques (PTM) challenged with SARS-CoV-2.
Radiographs were obtained prior to SARS-CoV-2 infection and at weeks 1-, 2-, and 5-weeks post infection (wpi). Baseline was established at 2 weeks prior to SARS-CoV-2 inoculation.

Cytokines

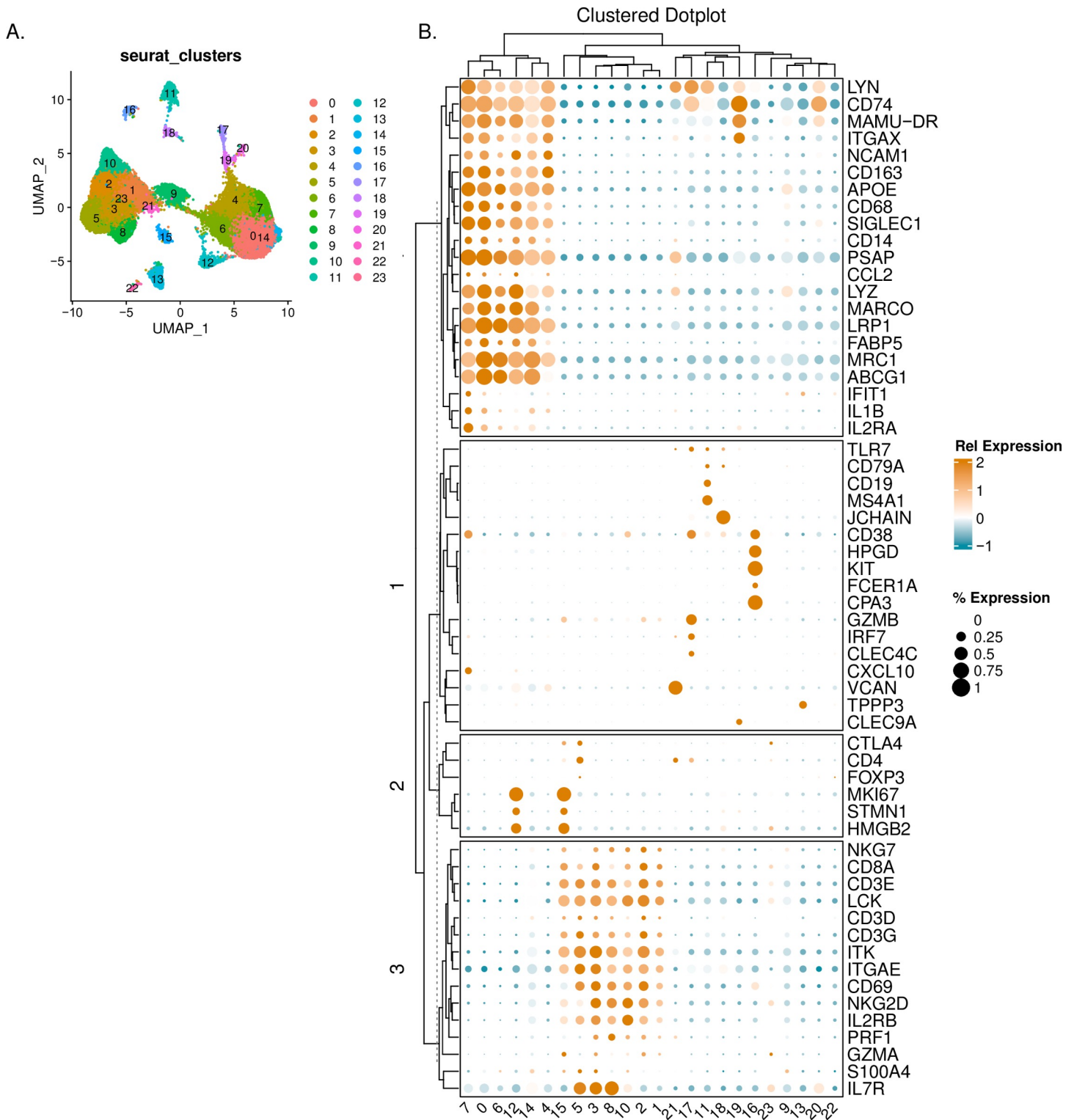


Supplemental Figure 3. Meso Scale analysis of cytokine and chemokine fluctuations in blood and BAL in PTM coinfected with SIV and SARS-CoV-2. A-C. Line graphs illustrating cytokine, proinflammatory cytokine, and chemokine dynamics in BAL supernatant and plasma before and 2-, 7-, 14-, 21-, 28-, and 42-days post SARS-CoV-2 infection.

A. CD4+ T cells



Supplementary Figure 4. Peripheral SARS-CoV-2 specific T cell responses were undetectable 21-days-post-infection. Two female pigtail macaques (PTM, NV18 & NV19) co-infected with SIVmac239 and SARS-CoV-2 shown. **A&B.** Flow cytometry dot plots demonstrating the IFN- γ and TNF- α response of CD4+ (**A**) and CD8+ (**B**) T cells to overnight SARS-CoV-2 peptide (spike, membrane, and nucleocapsid) stimulation. No Stim = cells incubated overnight without peptide stimulation.

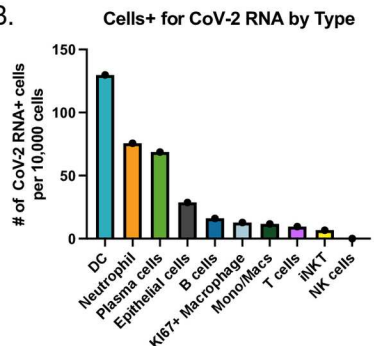


Supplementary Figure 5. Defining Seurat clusters. **A.** UMAP displaying Seurat-derived clusters obtained from FindAllMarkers function in Seurat. **B.** Dot plot depicting markers used to identify cell types. Hierarchical clustering method (hclust) was used to cluster columns and rows. The color of the dots indicates the relative gene (Rel. Expression). Dot size represents the percentage of cells expressing the gene (% Expression).

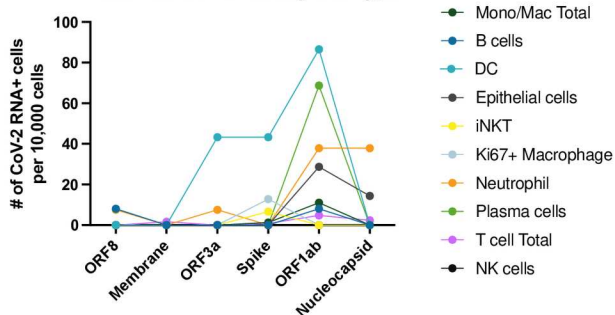
A.



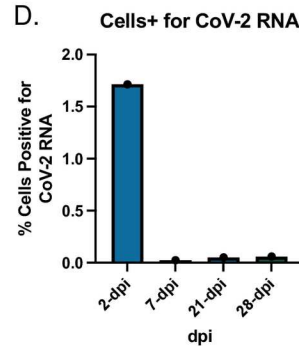
B.



C. Cells+ for CoV-2 RNA by Cell Type

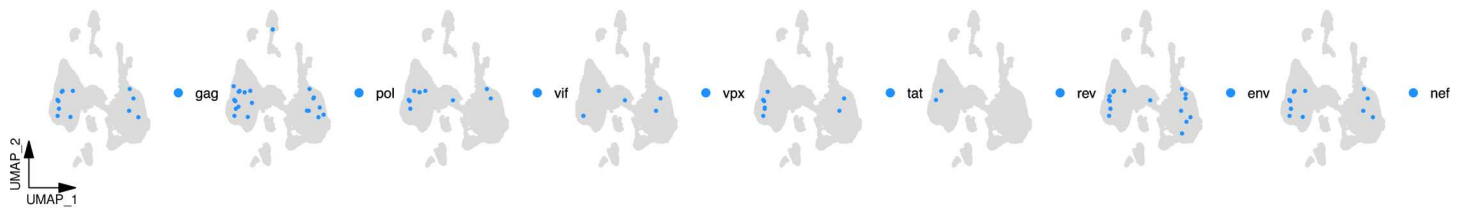


D.



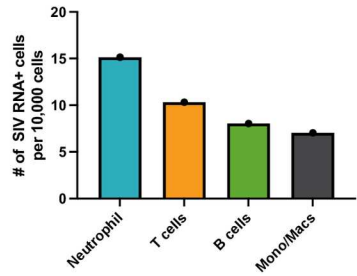
Supplemental Figure 6. Single-cell analysis of SARS-CoV-2 positive cells in BAL of SIV+ PTM. A. UMAP plots highlighting cells with detectable SARS-CoV-2 transcripts. **B.** Distribution of cells by cell type positive for any SARS-CoV-2 transcript. **C.** Number of cells positive for specific SARS-CoV-2 transcripts grouped by cell type. **D.** Percentage of cells positive for SARS-CoV-2 transcripts by days post-infection (dpi).

A.



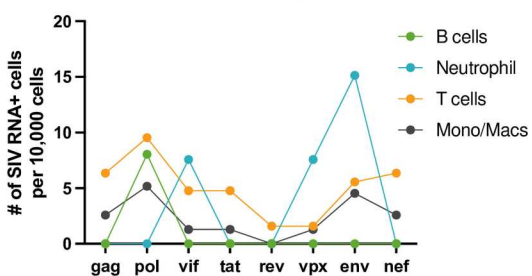
B.

Cells+ for SIV RNA by Type



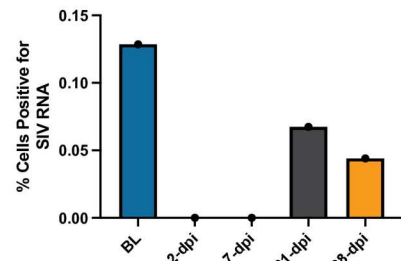
C.

Cells+ for SIV RNA by Cell Type

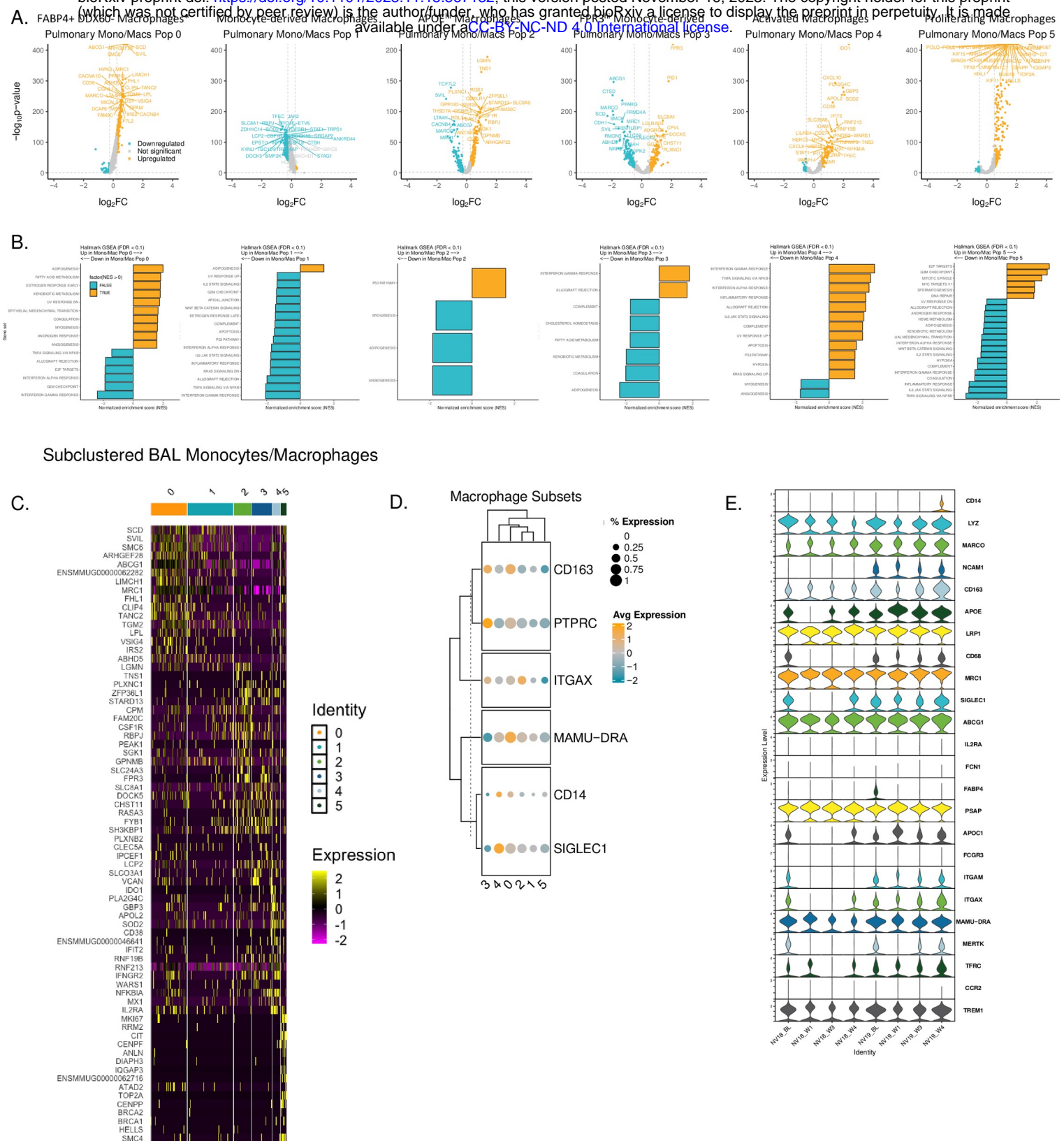


D.

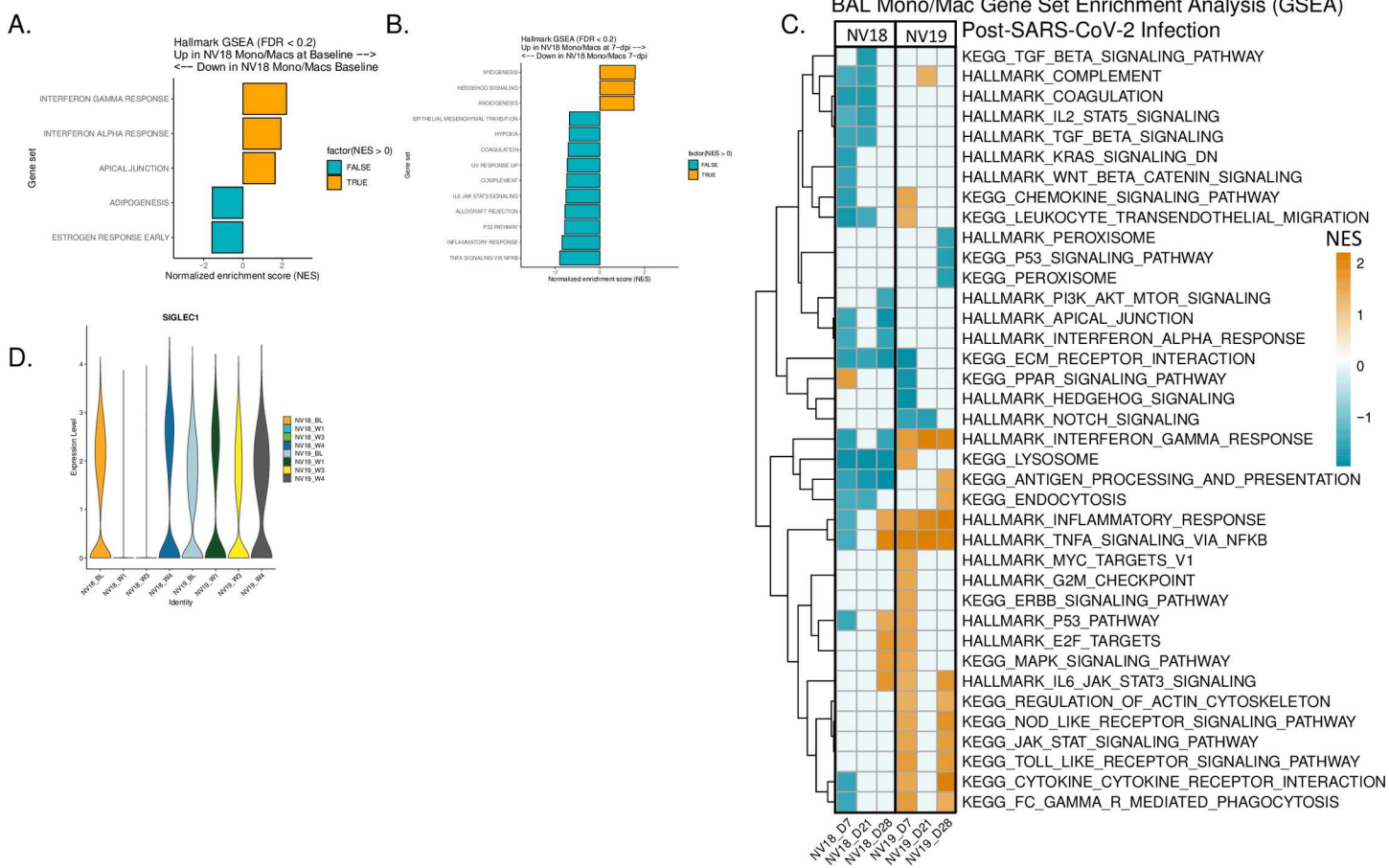
Cells+ for SIV RNA



Supplemental Figure 7. Single-cell analysis of SIV positive cells in BAL of coinfecting PTM. **A.** UMAP plots highlighting cells with detectable SIV transcripts. **B.** Distribution of cells grouped by type exhibiting any SIV transcripts. **C.** Number of cells positive for specific SIV transcripts grouped by cell type. **D.** Percentage of cells positive for SIV transcripts by days exposure.



Supplementary Figure 8. Single-cell monocyte/macrophage characterization. **A.** Volcano plots displaying significantly upregulated and downregulated differentially expressed genes (DEGs) in the Monocyte/macrophage populations. **B.** Bar plots depicting normalized net enrichment score (NES) from gene set enrichment analysis (GSEA) of Hallmark biological pathways. A false discovery rate (FDR) cutoff of 0.1 was used to determine significance. **C.** Heatmap of top 10 differentially expressed genes for each monocyte/macrophage cluster. **D.** Dot plot illustrating gene expression differences among the Seurat-derived clusters, corresponding to markers used in flow cytometry analysis (Figure 4 panel K). Hierarchical clustering (hclust) was used for column and row clustering. Dot color represents relative gene expression (Rel Expression), while dot size indicates the percentage of cells expressing the gene (% Expression). **E.** Stacked violin plot illustrating gene expression patterns of monocytes/macrophages at baseline (BL) and weeks 1, 3, and 4 post-SARS-CoV-2 infection.



Supplemental Figure 9. Differential gene expression (DEG) and enrichment analysis of Monocyte/Macrophage Subsets in NV18 and NV19. A&B. Gene set enrichment analysis (GSEA) of DEGs comparing NV18 and NV19 at baseline (A) and 7-dpi (B). **C.** GSEA results comparing DEGs at days 7, 21, and 28 post-exposure to baseline. A false discovery rate (FDR) cutoff of 0.2 was used to determine significance. **D.** CD169 (*SIGLEC1*) expression kinetics.